Global and Planetary Change 264 (2026) 105555

Contents lists available at ScienceDirect

Global and Planetary Change

journal homepage: www.elsevier.com/locate/gloplacha

Glacier changes in Langtang Catchment, Central Nepalese Himalaya from the Little Ice Age (~1815 CE) to 2023 CE

Gunjan Silwal [a,*], Bethan Davies [a], J. Rachel Carr [a], Owen King [a], Sammie Buzzard [b], Jonathan L. Carrivick [c], Prashant Baral [d]

[a] *School of Geography, Politics, and Sociology, Newcastle University, UK*
[b] *School of Geography and Natural Sciences, Northumbria University, UK*
[c] *School of Geography and water@leeds, University of Leeds, UK*
[d] *International Centre for Integrated Mountain Development (ICIMOD), Kathmandu, Nepal*

A R T I C L E I N F O

Editor: Aparna Shukla

Keywords:
LIA
Glacier area change
Elevation-dependent warming
Glacier fragmentation and disconnection

A B S T R A C T

Himalayan glaciers have experienced significant area and mass loss since the end of the Little Ice Age (LIA; ~mid-1800s to early-1900s), yet analysis of the patterns of recession and long-term, catchment-scale records remain scarce. Here, we reconstruct the extent and surface of glaciers at the LIA (~1815 CE) in the Langtang Catchment, Nepal Himalaya, using geomorphological indicators and Balanced-Ratio (BR) method, and quantify the long-term (LIA-1964/2023 CE) and recent (1964 to 2023 CE) changes in glacier extent based on Corona (1964/1974) and Sentinel (2016/2023) imagery, while examining climatic, topographic, and glaciological controls. Between the LIA and 2023, total glacier area decreased by 78.46 ± 4.38 km^2 (~41.5%), while glacier numbers nearly doubled from 58 to 115 due to separation, fragmentation, and disconnection. Glacier area loss rates increased more than fourfold, from 0.11% a^{-1} (LIA:1815–1964) to 0.49% a^{-1} (1964–2023) with further acceleration after 2000 (~0.79% a^{-1} during 2000–2016 and ~ 0.5% a^{-1} during 2016–2023). Glaciers in the catchment experienced widespread thinning, reduced flow velocities, and rising equilibrium-line altitudes (ELAs), coinciding with pronounced elevation-dependent warming (~0.3 °C dec^{-1} > 4000 m compared to 0.1 °C dec^{-1} at 3865 m a.s.l.; 1964–2023). Thinning progressively migrated up-glacier into accumulation zones, while rising ELAs increasingly intersected thinned and heavily crevassed icefall regions, driving glacier fragmentation and disconnection. Fragmented glaciers showed higher area loss, thinning rates, and reduced surface velocities, whereas disconnections in valley glaciers led to stagnation and degradation of debris-covered tongues. Our study highlights the critical need to assess glacier fragmentation and disconnection across the Himalaya. With enhanced warming at higher elevations, fragmentation and disconnection will likely become dominant mode of glacier recession in the region, with significant implications for future glacier evolution, meltwater availability, regional hydrology and associated geohazards.

1. Introduction

Himalayan glaciers cover ~22,800 km^2 (Bolch et al., 2012) and store ~3,000 km^3 of ice (Farinotti et al., 2019). Together with glaciers of the Hindu Kush, Karakoram, and Pamir ranges of High Mountain Asia (HMA), they sustain ten major transboundary river systems in Asia, directly supplying freshwater to over 240 million people and supporting the livelihoods of 1.65 billion people further downstream, particularly during dry seasons and droughts (Lutz et al., 2022). These glaciers also serve as crucial hydrological buffers supporting ecology, agriculture, and hydropower generation (Azam et al., 2018; Immerzeel et al., 2020; Lutz, 2016). However, since the end of the Little Ice Age (LIA), Himalayan glaciers have undergone substantial retreat and mass loss (Lee et al., 2021). This trend has accelerated in recent years due to pronounced thinning, fragmentation, and terminus recession driven by rising air temperatures and increasingly erratic precipitation patterns (Bhattacharya et al., 2021) and is expected to persist in the coming decades and century with enhanced warming rates at higher elevations (Fox-Kemper and Aðalgeirsdóttir, 2023; Jackson et al., 2023). These changes threaten the Himalayan cryosphere's ability to sustain river

* Corresponding author.
E-mail address: g.silwal2@newcastle.ac.uk (G. Silwal).

https://doi.org/10.1016/j.gloplacha.2026.105555
Received 17 February 2026; Received in revised form 27 May 2026; Accepted 3 June 2026
Available online 8 June 2026

flows and downstream water availability, particularly during dry seasons and in climatically drier western region due to changing glacier melt contributions to seasonal runoff (Immerzeel et al., 2020; Lutz, 2016).

Beyond water security and hydrological shifts, the retreat of Himalayan glaciers poses cascading ecological, economic, and societal risks. Shrinking glaciers threaten energy supply, local tourism, and mountain livelihoods (Immerzeel et al., 2020; Molden et al., 2022; Wester et al., 2019), while simultaneously amplifying cryospheric hazards, including slope instability and glacial lake outburst floods (GLOFs) (Carrivick and Tweed, 2016; Harrison et al., 2018; Zheng et al., 2021). The rapid growth of proglacial lakes and the progressive weakening of unconsolidated moraine dams are of particular concern, as they substantially increase the probability and potential magnitude of catastrophic GLOF events (Remya et al., 2019, 2025; Shrestha et al., 2023). Recent studies have reported increasing frequency of GLOFs across the Himalaya leading to significant loss of life and property (Allen et al., 2022; Mir et al., 2025; Sattar et al., 2025), alongside increased slope destabilization, sediment transport, and altered river channel morphology (Zhang et al., 2023). Deglaciation-driven changes in hydrological regimes and high-elevation microclimates further endanger specialized proglacial habitats and endemic mountain biodiversity, accelerating ecological degradation while facilitating the emergence of novel ecosystems (Bosson et al., 2023; Losapio et al., 2025). Continued deglaciation will reduce the aesthetic value, environmental stability, and accessibility of high-mountain landscapes affecting tourism-dependent livelihoods and increasing losses of lives and infrastructures from cryospheric hazards (Rasul and Molden, 2019). Beyond quantifiable economic losses, glacier loss also triggers a deep cultural and spiritual crisis. For many mountainous indigenous communities, glaciers are sacred landscapes or the abodes of their deities, and their loss signifies irreplaceable erosion of spiritual identity and cultural heritage (Allison, 2015; Bussard and Reynard, 2023).

Decadal-scale observations of the Himalayan glaciers show widespread glacier retreat, with pronounced spatio-temporal variability driven by region's diverse and spatially variable climatology (Bhattacharya et al., 2021; Fujita and Nuimura, 2011). This variability is further modulated by differences in glacier type and distribution (Bajracharya et al., 2014, 2015), as well as glacier geometry and morphology (King et al., 2018, 2020). Understanding these spatial and temporal patterns is critical for identifying regional controls on glacier dynamics and for effectively managing water resources and associated cryospheric hazards across the Himalaya (Bhattacharya et al., 2021; Jackson et al., 2023). Despite recent advances in Himalayan glaciology, major uncertainties remain in rates of ice loss, hydrological responses, and underlying climate drivers, largely due to a lack of long-term (centennial-scale) observations (Lee et al., 2021). Reliable projections of future glacier extent, evolution, and water-resource availability therefore require reconstructions of past glacier extents, improved constraints on long-term retreat rates (Reinthaler and Paul, 2025), and validation of glacier models over extended timescales (e.g., ~100 years; Carrivick et al., 2022, 2024). Accurate glacier inventories and historical maps are fundamental to robust mass-balance calculations and change assessments (Paul et al., 2013; Zemp et al., 2015); when integrated with local geomorphological and climatic records, they also provide valuable insights into past glacier dynamics (Benn and Evans, 2010).

Within the broader Himalayan context, the Central Himalaya represents a key climatic transition zone where interactions between the Indian Summer Monsoon and mid-latitude westerly disturbances strongly influence glacier behaviour (Azam et al., 2018; Jackson et al., 2023). Geochronological evidence documents widespread late Holocene and the LIA glacier advances in this region, with some glaciers remaining close to their maximum extents into the early twentieth century despite substantial mass loss (Rowan, 2017; Shekhar et al., 2017). However, the limited availability of spatially distributed data, particularly documenting the transition from the LIA maxima to present-day glacier extents constrains assessments of how glacier characteristics modulate climatic responses. This study therefore aims to address this gap by quantifying glacier area changes in the Langtang Catchment, Central Nepal Himalaya, from the LIA to 2023 using multi-temporal and multi-source datasets, to establish a baseline for understanding long-term and recent glacier changes in the Himalayas. The objectives of this study are to i) reconstruct LIA glacier extents and surface ii) analyse both long-term (LIA-1964/2023) and satellite-era (1964–2023) glacier changes, and iii) quantify the drivers of glacier changes in the Langtang Catchment.

2. Study site

The Langtang Catchment (28.08°to 28.38°N and 85.34° to 85.79°E) is located in the Rasuwa district, Central Nepal Himalaya, about 70 km north of Kathmandu (Fig. 1a). It stretches from the summit of Langtang-Lirung (7246 m a.s.l.) to the town of Syafrubesi (1400 m a.s.l.), at the confluence of the Langtang River and the Trishuli River (Fig. 1b). Within this elevation range, the catchment covers an area of 585 km^2, ~ 21.5% (125 km^2) of which is glacierized (Steiner et al., 2021). More than 70% of the glacial mass is found within the elevation range of 5000 and 5800 m a.s.l. and extensive debris cover is present below ~5400 m a.s.l., on the ablation zones of the valley glaciers (Fig. 1d). Langtang Glacier is the largest, covering ~57.45 km^2 in 2000 CE (RGI Consortium, 2023), with 15.5 km^2 of debris-covered tongue extending below 5400 m a.s.l. (Ragettli et al., 2016).

The climatology of the catchment is influenced by the Asian summer monsoon, with synoptic-scale easterly winds dominating in summer (June to September) and mid-latitude westerly extratropical winds in winter (October to May) (Steiner et al., 2021). Mean annual precipitation and temperature in the catchment recorded at the Kyanjing automatic weather station (AWS) at 3862 m a.s.l. (Fig. 1b) by Department of Hydrology and Meteorology (DHM) were ~ 680 mm and 3.2 °C, respectively, for 1988 to 2016 CE (Fig. 1c). The catchment receives ~70–90% of its annual precipitation during the monsoon but varies from ~2000 mm at 2300 m a.s.l. to ~1000 mm at 3900 m a.s.l. (Immerzeel et al., 2014). Monsoon-driven moisture and cloud cover influence snow accumulation and melt, making the catchment's glaciers 'summer-accumulation type' (Ageta and Higuchi, 1984; Stumm et al., 2021).

Glacial geomorphological evidence indicates that the Langtang Valley reached its most extensive mid-Holocene glaciation around ~3650 to 3000 ^{14}C yr BP, when the Lirung Glacier extended to the Langtang Village ~3400 m a.s.l., based on radiocarbon dating (Shiraiwa and Watanabe, 1991; Fig. 1b). The most recent major glaciation occurred during the LIA, with two major advances. The Yala I advance is dated to ~1350–1480 CE (Barnard et al., 2006) constrained by terrestrial cosmogenic nuclide (TCN) and radiocarbon dating methods. However, Shiraiwa and Watanabe (1991) could not constrain the age of Yala I stage, but they suggested that this might correspond to the LIA in Langtang Valley. This timing is consistent with the peak moraine building of LIA (1300–1600 CE), in the Himalaya (Rowan, 2017). The latest maximum advance, Yala II occurred ~1910 CE (40 ± 130 cal. yr. BP; Shiraiwa and Watanabe, 1991), constrained by ^{14}C dating method, although Ono (1985) estimated the age of ~1815 CE based on till-fabric and annual ridge analyses of Yala Glacier.

3. Data and methods

3.1. Data and data sources

To quantify glacier changes in the Langtang Catchment over both long-term (LIA, ~ 1815 to 1964/2023 CE) and recent (1964 to 2023 CE) periods, we used high-resolution satellite images acquired at multiple dates. Glacier extents for 1964 and 1974 were mapped using georeferenced and co-registered declassified Corona KH-4 (~5 m

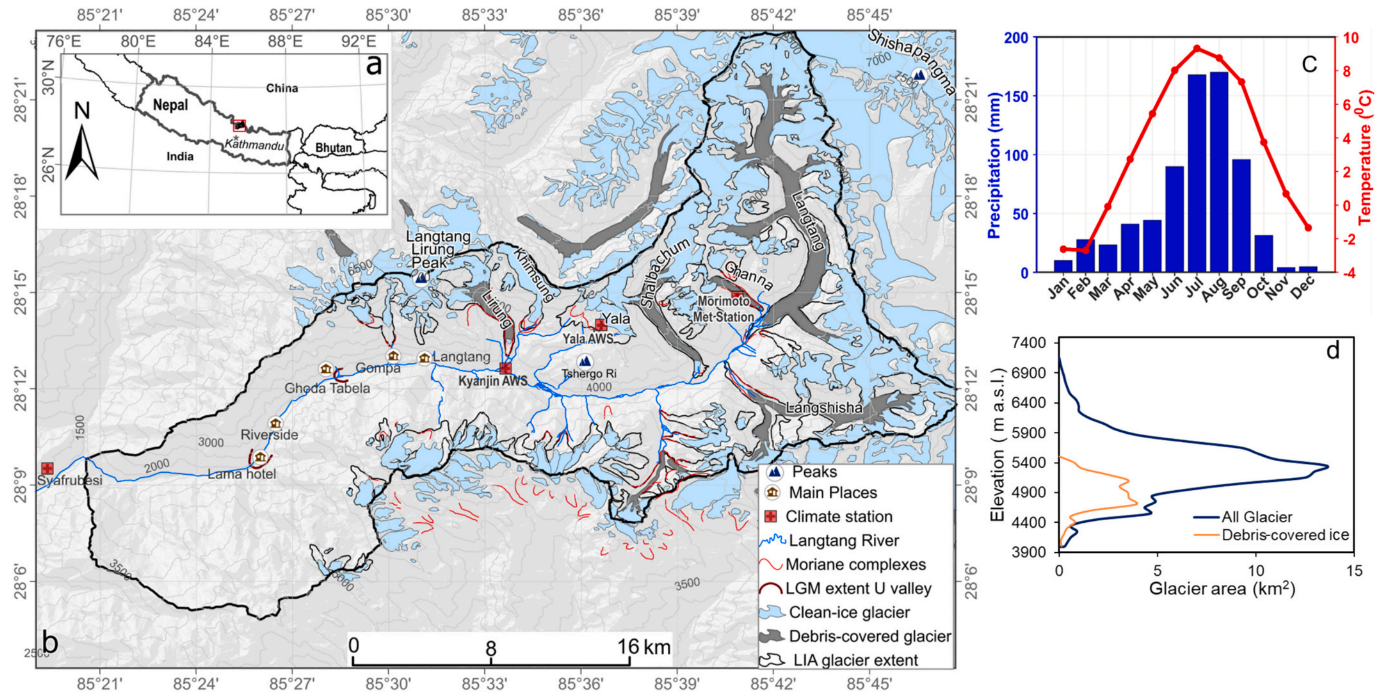

Fig. 1. (a) Location of the study area, Langtang Catchment (highlighted by the red rectangular box), (b) a detailed map of the Langtang Catchment, with placemark for major places, meteorological stations, and peaks. The major glacier systems in the catchment are labelled on the map, the LGM extent (U valley in brown) and moraine complexes in red solid lines are digitized from Shiraiwa and Watanabe (1991). Glacier outlines (sky-blue polygons) are from RGI v.7.0, while debris-covered glacier outlines (light grey polygon) are from ICIMOD glacier inventory (https://rds.icimod.org). (c) the climatology (temperature and precipitation from 1988 to 2016) is from Kyanjing station (3862 m a.s.l.) and (d) the hypsometric curve of the glaciers (all glacier in solid dark blue line and debris-covered ice in orange solid line) based on RGI v.7.0 glacier outlines (for all glaciers) and ICIMOD glacier inventory (for debris-covered glaciers) and Shuttle Radar Topography Mission (SRTM GL1) Global 30 m void-filled DEM from 2000 (Farr et al., 2007). (For interpretation of the references to colour in this figure legend, the reader is referred to the web version of this article.)

resolution) and Hexagon KH-9 (~7 m) imagery, respectively, sourced from the study of Bhattacharya et al. (2021). Glacier extents for 2016 and 2023 were derived from Sentinel-2 A and Sentinel-2B multispectral imagery (10 m). All images used for mapping (Supplementary Table S1) were acquired during November and December, with minimal snow and cloud cover. We used RGI v7.0 glacier outlines (~2000 CE; RGI Consortium, 2023) as a baseline; these were thoroughly cross-checked and corrected for any misalignments and mapping errors (Supplementary Fig. S1) prior to their use in reconstructing the LIA extent and delineating glacier boundaries for the years:1964, 1974, 2016, and 2023. These corrected RGI glacier outlines from ~2000 CE were also utilized for glacier change analyses for the year 2000 CE. For debris-covered glaciers, shapefiles from the ICIMOD glacier inventory (census date ~2005 ± 3 years; https://rds.icimod.org) were used as reference and debris cover outlines were manually edited for each mapped year by overlaying the outlines on contemporaneous satellite imagery.

The Shuttle Radar Topography Mission (SRTM GL1) Global 30 m void-filled DEM from 2000 CE (Farr et al., 2007) was used for generating topographic parameters (elevation, aspects, slope, hillshade). To assess recent glacier changes in the catchment, we utilized elevation change data (2000–2019 CE) of Hugonnet et al. (2021) and annual median velocity fields (1988 to 2022 CE) from the ITS_LIVE archive (Gardner et al., 2022). Additionally, we used ERA5-Land reanalysis (~9 km × 9 km resolution) daily temperature and precipitation (1960 to 2023 CE) to examine the climatology of the catchment over the period. All datasets used in this study are summarized in Supplementary Table S1.

3.2. Little Ice Age (LIA) glacier surface and extent reconstruction

We combined geomorphological indicators including trimlines, moraine crests, and debris cover extent with RGI v7.0 glacier outlines to reconstruct LIA glacier extent. Geomorphological indicators were identified following established criteria for different glacierized regions of the globe (e.g. Carrivick et al., 2019, 2020, 2022, 2024; Glasser et al., 2005) on Sentinel-2 A and 2B satellite imagery from 2016 and 2023, overlain on a hillshade of the SRTM DEM. High-resolution 3D images from Google Earth and the sub-meter resolution WorldView/GeoEye imagery available from Maxar within ESRI ArcGIS Pro 3.1, further supported the mapping of lateral and terminal moraine crests and trimlines. The outer, highest, often continuous and clearly visible moraine crests down-valley of contemporary glacier termini were digitized as the LIA maximum (Reinthaler and Paul, 2023). For glaciers which lacked distinct geomorphological evidence and moraine complexes featuring multiple inconsistent crests, we relied on published records of late quaternary glacial fluctuations in the Langtang Valley (Shiraiwa and Watanabe, 1991; Supplementary Figs. S2a–d & Fig. 1b). These records indicated that the innermost moraine complex (Yala I) to be the latest maximum glacier extent in the catchment, and this was adopted as the LIA boundary in ambiguous cases.

The LIA extents were finally digitized by modifying RGI v.7.0 outlines in ArcGIS Pro 3.1 along trimlines and moraine crests interpreted to represent the LIA maximum identified on satellite imagery and Maxar WorldView/GeoEye, following Reinthaler and Paul (2023) and Davies et al. (2024). These geomorphological interpretations were validated during a November 2024 field campaign, where terminus positions, debris extent, and moraines were ground-truthed for selected glaciers. To corroborate the historical extents, we also consulted aerial imagery (1976–1978), archived at https://ads.nipr.ac.jp/data/ (Supplementary Figs. S3a-d). The uncertainty in LIA extent area was calculated following Reinthaler and Paul (2023), which considers uncertainty arising from manual digitization of LIA extent as well as from interpretation of geomorphological indicators (see Supplementary Section 5 for the details).

Reconstruction of LIA surface was limited to ablation zones due to the absence of moraines and clear trimlines above the ELA. For this, we first estimated glacier-specific LIA ELAs using Balanced Ratio (BR) method of Pellitero et al. (2015). We applied an average value (BR = 1.56) suitable for paleo-glaciers following Oien et al. (2022). The glacier-specific LIA ELAs were then subsequently merged with the mapped moraine crests and trimlines to create ablation area polygon for each glacier, which were then extracted in an automated fashion following Carrivick et al. (2019, 2020, 2022, 2024). The vertices of each ablation area were then converted to points to enable extraction of elevations of the terminal and lateral moraine crests and of ELA from a DEM. We used 30 m SRTM DEM because the DEM choice including their resolution and dates have a negligible effect, compared to uncertainty in timing of LIA, in calculations of rates of glacier change (cf. Carrivick et al., 2019, 2020, 2022, 2024). The LIA surface for ablation zone was then reconstructed by interpolating the elevations between these points with elevation values. The natural neighbour interpolation method was applied as per the recommendation of Carrivick et al. (2019, 2020).

We used this reconstructed glacier surface during LIA to calculate the long-term volume change in the Langtang Catchment. However, volume change could only be calculated between the LIA and 2000 CE due to the DEM availability. For this, we first calculated the surface lowering by differencing the reconstructed LIA surface with SRTM DEM from 2000 CE. This surface lowering was then converted to a glacier-specific volume change by summing up all the negative values (representing surface lowering) and multiplying those by the cell size of the DEM (30 × 30 m), from which we derived mean annual change rate. The inferred LIA positions and volume change for Langtang catchment from this study were also checked against the published LIA extent and volume change of Lee et al. (2021) for HMA who used RGI v6.0 glacier outlines as their base for LIA extent reconstruction and a slightly higher balance ratio (BR = 1.75) for LIA ELA reconstruction. We found negligible differences between our LIA extent and estimated volume change and those reported by Lee et al. (2021).

3.3. Glacier mapping, area change analysis and uncertainty

Glacier outlines of all glaciers for 1964, 1974, 2016, and 2023 were manually delineated from declassified Corona and Hexagon imagery, and Sentinel scenes, respectively, using corrected RGI v7.0 (~2000 CE), with debris-covered areas cross-referenced against ICIMOD's inventory of debris-covered extents (~2005 CE). Manual delineation of both clean-ice and debris-covered glaciers was enabled by the sufficient contrast between glacier and land-cover in panchromatic KH-4/KH-9 and band combinations of RGB, NIR, and SWIR1 for Sentinel-2 A and 2B images.

For glacier area change assessment, the RGI v7.0 outlines were overlain on declassified and Sentinel imagery following established methods (Bolch et al., 2010; Bhambri et al., 2011). Glacier outlines were then manually edited according to observed changes around the glacier margin for each period from the respective year's imagery, both in the terminus and forefield areas. These multi-temporal datasets were then used for calculating absolute and relative area change rates across five distinct intervals: LIA–1964, 1964–1974, 1974–2000, 2000–2016, and 2016–2023. We retained original RGI IDs for each glacier polygon and where glaciers had separated into multiple polygons from their parent glacier, the same RGI ID was used for all polygons to facilitate subsequent comparison following Davies et al. (2022). Each glacier polygon was further categorized as valley, cirque, plateau, hanging, simple basin, and niche (Supplementary Fig. S4) following Bajracharya and Shrestha (2011). With these mapped glacier outlines, we calculated absolute (km^2) and relative (%) glacier area change, annual rates of change in terms of absolute area change per annum ($km^2\ a^{-1}$), proportional rates of area change ($\%\ a^{-1}$), and mean rate of change ($km^2\ a^{-1}$) for all glaciers in the catchment for both long-term (LIA to 1964) and recent (1964 to 2023) periods.

For the long-term glacier area change assessment, we set the LIA age as ~1815 CE (~208 years prior to 2023), corresponding to LIA maximum of Yala Glacier based on annual moraine-ridge analyses (Ono, 1985). Dating of LIA maxima across the Himalaya remains limited to a small number of glaciers, and where dated, LIA maxima exhibit spatially variable timing, with many glaciers reaching their maximum extents during the late 19th to early 20th centuries depending on size, hypsometry, and local climate (Owen et al., 1998; Rowan, 2017; Shekhar et al., 2017; Grove, 2019). We, therefore, used 1815 CE as a reference age consistent with Kayastha and Harrison (2008), who applied this timing for regional equilibrium line altitude reconstructions across the Nepal Himalaya. This date is further corroborated by tree-ring reconstructions from Nepal (Cook et al., 2003), who recorded a sustained temperature increase after ~1825 CE, indicating that climatic conditions favourable to glacial advance had effectively ceased by this time.

Uncertainty in glacier surface area was calculated following methods described by Davies et al. (2022, 2024) and Paul et al. (2013). Ten representative glaciers, across the spectrum of glacier sizes and including both debris-covered and clean-ice glaciers were digitized 5 times on Corona KH4, Hexagon KH9 and Sentinel 2 A and 2B imagery for each year, with 2–3 days between each round of digitizing (Supplementary Fig. S3). The mean, relative standard deviation (RSD) and 95% confidence interval of glacier area was then calculated for each glacier (Supplementary Table S2). A regression through the data points (mean glacier area and 95% confidence interval; $r[8] = 0.91$, $p < 0.001$) provided an equation that was used for size-specific up-scaling of the 95% confidence interval to the full dataset, which was used as the uncertainty in glacier area following Davies et al. (2022, 2024). See section 5 of Supplementary material for the details.

3.4. Glacier attributes (elevation, slope, aspect, and hypsometry)

The characteristics of glacier distribution were examined by statistically analyzing the relations between topographic and hypsometric parameters and glacier area. For this, we derived mean glacier slope, aspect and minimum (Z_{min}), maximum (Z_{max}), mean (Z_{mean}), and median (Z_{med}) elevations for each glacier from void filled SRTM 30 m DEM and 2023 glacier outlines with zonal statistics. The hypsometric index (*HI*) was calculated following Jiskoot et al. (2009) and Mcgrath et al. (2017).

$$HI = \frac{(Z_{max} - Z_{med})}{(Z_{med} - Z_{min})} \quad (1)$$

But if $0 < HI < 1$, then.

$$HI = \frac{-1}{HI} \quad (2)$$

The *HI* indices were grouped into very top-heavy ($HI < -1.5$), top-heavy ($-1.5 < HI < -1.2$), equidimensional ($-1.2 < HI < 1.2$), bottom-heavy ($1.2 < HI < 1.5$), and very bottom-heavy ($HI > 1.5$). Top-heavy glaciers have their area distribution strongly skewed toward the top of their elevation range (Davies et al., 2022).

3.5. Glacier disconnection, fragmentation, and separation

We mapped glacier disconnections, separations, and fragmentations of glaciers across all imagery for each time period. Disconnections were mapped where a glacier flow unit, defined by flowlines, has become disconnected in the along-flow direction, separating the ablation area or glacier tongue from its accumulation area which formerly supplied ice (Davies et al., 2022, 2024; Rippin et al., 2020; Supplementary Fig. S5b). Disconnections occurred mostly at the steep and thinned icefall areas formed at topographic steps with bare rock areas or bedrock exposed. Terminus separations were mapped on the valley floor where previously connected tributary glaciers were completely severed from the trunk glaciers, typically in large valley glaciers where tributary glaciers experience extensive retreat compared to its main trunk. Separations do not occur over bedrock steps, and do not separate accumulation and ablation areas (Davies et al., 2022; Supplementary Fig. S5c). Glacier fragmentation was identified where glaciers broke into smaller units due to significant lateral shrinkage and thinning (Supplementary Fig. S5a). Fragmentation and disconnections are often accompanied by bedrock exposure between the fragmented glacier units (Davies et al., 2022). These features were mapped where visible in the glacier outlines between 1964 and 2023, and where structural glaciology (e.g., flowlines) and geomorphology (e.g., moraines, trimlines, bedrock lineation) indicated formerly confluent ice-flow.

3.6. Glacier equilibrium line altitude (ELA) and mass balance (MB)

To assess the glacier evolution in the Langtang Catchment and evaluate the role of climatic drivers, particularly of temperature and precipitation for recent period, we analyzed changes in glacier MB and ELA between 1960 and 2020. We computed ELA and MB of individual glaciers in the Langtang catchment using Open Global Glacier Model (OGGM; Maussion et al., 2019) at an annual resolution. Glacier MB in OGGM is computed with the extended version of a temperature index model using monthly precipitation and temperature data optimized with temperature sensitive and precipitation phase partitioning parameters. These parameters are calibrated using glaciers with specific mass balance observations (Marzeion et al., 2012, 2020). We used the standard baseline GSWP3-W5E5 data (Lange et al., 2021), as implemented in the OGGM to simulate MB. The monthly mass balance (m_i) at elevation (z) for any month in OGGM is computed as:

$$m_i(z) = {}_{pf}P_i^{solid}(z) - \mu^* max\left(T_{i(z)} - T_{melt}\, , 0\right) + \mathcal{E} \tag{3}$$

where, pf is global precipitation correction factor ($pf = 2.5$ or variable), P_i^{solid} is solid precipitation, μ^* is glacier temperature sensitivity factor that needs to be calibrated, T_i is air temperature, T_{melt} is the melt temperature at which glacial ice melt occurs. We set $T_{melt} = 0^{\circ}C$, so the amount of solid precipitation is expressed as a percentage of total precipitation: 100% solid precipitation occurs if $T_i \le 0$ $(0^{\circ}C)$, no solid precipitation if $T_i \ge 2$ $(0^{\circ}C)$. The precipitation is linearly interpolated for $T_i \le 0$ *and* $T_i \ge 2$. $\mathcal{E}$ is the residual bias term added as a tuning parameter to represent the collective effects of non-climatic factors (Maussion et al., 2019). The modelled MB was calibrated with available geodetic MB of Hugonnet et al. (2021) for individual glacier after 2000 (see Supplementary Section 4.2.1). The ELA was then determined as the elevation where the net annual mass balance equals zero ($b(zELA) = 0$). Finally, we calculated the regional mean ELA and mass balance for the Langtang Catchment based on the individual glacier estimates and their respective areas.

3.7. Glacier surface velocity and surface elevation change

We incorporated glacier surface velocity fields generated as part of the ITS_LIVE project (Gardner et al., 2018, 2022) into our analyses to better understand the changes in glacier dynamics in the Langtang Catchment from 1988 to 2020, alongside changes in glacier area for the recent period. ITS_LIVE dataset is composed of median surface velocity fields that cover 95% of glacier area across HMA over the period 1985–2023 (Dehecq et al., 2019; Gardner et al., 2022). The annual median velocity fields are derived from a stack of velocity fields generated from multiple individual pairs of Landsat scenes using the AUTO_RIFT algorithm (Gardner et al., 2022). We used glacier average annual median velocity in our analyses. We further used surface elevation change estimates derived from DEM differencing for the recent period (2000–2019) based on Hugonnet et al. (2021) to determine the glacier thinning rates in the catchment alongside the changes in glacier surface velocity.

3.8. Climate trends

To evaluate the climatological drivers of glacier change in the Langtang Catchment, we utilized ERA5-Land (9 × 9 km) near-surface (2 m) air temperature and total precipitation data from 1960 to 2023, extracted for the glaciated areas of the catchment (~4000–6500 m a.s.l.). ERA5-Land is produced by rerunning the ECMWF land surface model forced by ERA5 meteorological fields (Muñoz-Sabater et al., 2021). To correct the effect of topographic smoothing over complex terrain, the temperature and precipitation data were downscaled to median glacier elevation using catchment-specific lapse rates and precipitation gradients (Immerzeel et al., 2014), with ERA grid cell surface elevations derived from geopotential height divided by the acceleration due to gravity. We further compared the downscaled ERA5-Land data with in-situ observations from the Kyangjin AWS (3865 m a.s.l.) for the overlapping period 1988–2016 (Supplementary Fig. S6 and Table S3). Evaluation using Pearson correlation coefficient (r) and root mean squared error ($RMSE$) demonstrated strong agreement for both ($r = 0.90$ and $RMSE = 4.8$) and precipitation ($r = 0.79$ and $RMSE = 156.5$ mm).

4. Results

4.1. Glacier inventory and glacier area changes (LIA – 2023)

4.1.1. Glacier inventory and characteristics of glaciers in 2023 CE

In 2023, the Langtang Catchment contained 115 glaciers totalling 111.75 ± 2.11 km^2 (Table 1). Of these, eight (~7%) were debris-covered glaciers, characterized by thick, continuous mantles of sand, gravel, rocks covering 40–70% of their ablation areas (Supplementary Figs. S7a-c & Table S6). The debris-covered glaciers (including clean-ice above 5400 m a.s.l. and thick layer of supraglacial debris tongue below) covered ~61.20 ± 1.4 km^2 of total glacier area, of which the supraglacial debris tongue alone covered 31.03 ± 0.87 km^2, representing between ~18 and 50% of the total area of individual debris-covered glacier (Supplementary Table S6). The majority of glaciers (~84%) were smaller than 1 km^2, contributing ~25.3 km^2 (~23%) to the total glacierized area, while only 2.6% exceeded 10 km^2, but contributed to ~58 km^2 (~52%) of the total glacierized area (Fig. 2a). The glacier population comprised glacierets and hanging glaciers (~24% each), cirque (~18%), plateau (~15%), niche (~13%), simple basin (~8%), and valley glaciers (~4%) (Fig. 2b). Despite their small number (~4%), valley glaciers contributed the largest share of glacier area (~60%) (Fig. 2b).

Hypsometric index analyses showed that glaciers in the catchment were predominantly equidimensional (Equi: 30%), very top heavy (VTH: 21%), and top heavy (TH:19%) (Fig. 2c), mainly due to the presence of high elevation and small glacierets, hanging and cirque glaciers (Fig. 2b). However, in terms of area coverage, bottom heavy (BH) glaciers covered 45.89 km^2 (~41%) and very bottom-heavy (VBH) glaciers covered 19.47 km^2 (~17%) of the total 111.75 km^2, altogether making ~58% of the total glacier area (Fig. 2c). Large valley glaciers were either BH (e.g. Shalbachum) or VBH (e.g. Langtang, Langshisha).

Glacier sizes ranged widely, from 0.03 km^2 to 35.75 km^2 with mean size of ~1 km^2. Both glacier number and glacier area were predominantly oriented toward SE-SW aspects (Figs. 2d-e & Figs. 2f-g). Examples of glacier types and glacier size are shown in Supplementary Fig. S4. Mean glacier elevation ranged from 4245 m a.s.l. to 6760 m a.s.l. (Fig. 3a). Glaciers <2 km^2 had a higher mean elevation (~5620 m a.s.l.) compared with larger glaciers (≥5 km^2; 5100 m a.s.l.). The large valley glaciers (e.g. Langtang, Shalbachum, and Langshisha) spanned wide elevation ranges from ~4200 to 6800 m a.s.l. (≥2000 m), whereas smaller glaciers (<1 km^2) had an average elevation range of ~380 m (Fig. 3b).

The median elevation of glaciers in the catchment ranged from 4900 to 6780 m a.s.l. (an average of 5610 m a.s.l.; Fig. 3e). More than 70% of the total glacier area in 2023 was concentrated within this elevation range. The mean slope of all glaciers was ~30° (ranging from 9° to 69°, Fig. 3c) and varied greatly with their size. Valley glaciers with extensive debris tongues had gentler slopes (~10°), while hanging glaciers were

Table 1
Glacier area changes in the Langtang Catchment from LIA (a range of ages are used here to show the sensitivity of LIA timing in long-term area change rate calculations) to 2023. *Note that changes in debris covered extent was only computed during the recent period.

Year (CE)	Total glacier area (km^2)	Mean glacier area (SD), km^2	Count of glaciers	ΔArea (km^2)	Area change (%)	Total rate of glacier Δ Area ($km^2\ a^{-1}$)	Rate of glacier change ΔA (%a^{-1})	Mean rate of glacier change ($km^2\ a^{-1}$)
				Both clean-ice and debris-covered glaciers				
1300–1600[a] 1470 ± 1600[b] 1815 CE[c] 1823 ± 1900[d] 1900-1910[e]	190.21 ± 3.84	3.29 (9.75)	58					
1964	158.07 ± 2.66	2.08 (5.99)	75	−32.14 ± 4.67	−16.90 ± 2.35	−0.048 to −0.62 **−0.22**	−0.025 ± 0.0035 to −0.32 ± 0.045 **−0.11 ± 0.02**	**−0.003**
1974	151.07 ± 3.19	1.82 (5.60)	83	−7.00 ± 4.14	−4.43 ± 2.6	−0.7	−0.44 ± 0.26	−0.0089
2000 (corrected RGI v7.0 outline)	132.7 ± 3.32	1.45 (5.77)	100	−18.37 ± 4.60	−12.16 ± 3.0	−0.71	−0.47 ± 0.12	−0.0071
2016	115.83 ± 1.26	1.02 (3.69)	113	−16.87 ± 3.52	−12.71 ± 2.7	−1.05	−0.79 ± 0.17	−0.0093
2023	111.75 ± 2.11	0.97 (3.59)	115	−4.08 ± 2.40	−3.52 ± 2.08	−0. 58	−0.50 ± 0.30	−0.0051
Total change (LIA −2023)			+57	−78.46 ± 4.38	−41.25 ± 1.62	−0.11 to −0.69 **−0.38**	−0.057 ± 0.002 to −0.36 ± 0.014 **−0.2 ± 0.01**	**−0.0016**
Glacier area rate change for different periods during satellite era								
1964–2023			+40	−46.32 ± 3.40	−29.3 ± 2.15	−0.78	−0.49 ± 0.01	−0.0071
1964–2000			+25	−25.37 ± 4.25	−16.05 ± 3.2	−0.71	−0.45 ± 0.09	−0.0070
2000–2023			+15	−20.95 ± 3.9	−15.79 ± 2.9	−0.91	−0.69 ± 0.13	−0.0075
				*Debris-covered extent only				
1964	28.92 ± 0.98	4.44 (5.31)	6					
1974	28.95 ± 1.07	4.13 (5.22)	6	0.03 ± 1.45	0.072 ± 5.02	0.0021	0.007	0.0003
2016	31.75 ± 1.14	3.49(4.99)	8	2.8 ± 1.56	9.71 ± 5.4	0.067	0.23	0.0075
2023	31.03 ± 0.87	3.42(4.92)	8	−0.72 ± 1.43	−2.28 ± 4.52	−0.104	−0.33	−0.012
1964–2023	2.11 ± 1.77		2	2.11 ± 1.31	7.3 ± 4.53	0.036	0.12	0.0004

[a] LIA maximum age suggested by Rowan (2017) and used by Lee et al. (2021);
[b] LIA for Lirung Glacier representing Yala I, based on TCN dating method (Barnard et al., 2006);
[c] LIA for Yala Glacier based on annual moraine ridge analysis and is consistent with the post LIA temperature warming analyzed from annual tree ring datasets from Nepal Himalaya and also adopted in this study (values in bold) as a fixed age for area change rate comparisons;
[d] Minimum of Yala II, based on ^{14}C dating (Shiraiwa and Watanabe, 1991);
[e] Maximum of YalaII, ^{14}C dating (Shiraiwa and Watanabe, 1991), but they could not pinpoint the exact date because of the lack of good sample.

steeper (>35°) (Fig. 3h). Morphological type and spatial distribution of glacier size classes and their descriptive characteristics are reported in Supplementary Table S4a-b & Table S5.

4.1.2. LIA glacial extent and surface reconstruction and volume change (LIA ~1815–2000 CE)

Reconstructed LIA glacial extents totalled 190.21 ± 3.84 km^2 (n = 58), ~41% larger than the area observed in 2023 CE (Figs. 4a-d & Fig. 5; Table 1). The total area was dominated by a few large valley glaciers, as indicated by the highly skewed size distribution (mean glacier size of 3.29 km^2 and SD = 9.75; Table 1). Likewise, the large valley glaciers (e. g. Langtang and Langshisha) comprised multiple tributary glaciers merging to a single terminus. These glaciers extended at least a few hundred meters (~700 m for Langtang Glacier) to more than a kilometer (~1720 m for Langshisha Glacier) lower than their 2023 extent, forming a long, narrow, low-sloped glacier snout (Fig. 4d). Shalbachum Glacier, another valley glacier, extended down to the Langtang River, terminating in a broader snout (~540 m lower than the present, Fig. 4d & Fig. 5). The LIA extent was constrained by lateral and frontal moraines for valley glaciers, and by amphitheatre-shaped hollows on mountain flanks for cirque glaciers (Supplementary Figs. S2a-d). Glacier GL1 displayed a recessional moraine (Supplementary Fig. S2c), and in Lirung Glacier, moraine-dammed depressions are now infilled with proglacial lake water (Supplementary Fig. S2a).

By differencing the LIA surface with the 2000 SRTM DEM, we found that surface lowering exceeded ≥100 m in the central ablation areas of large valley glaciers, far up-glacier from the current termini (Fig. 4d). This thinning resulted in a total cumulative volume loss of 3.56 km^3 between the LIA and 2000. Thinning rates were greatest on Lirung (mean = −0.33 m a^{-1}, SD = 0.13), followed by GL1 (mean = −0.29 ma^{-1}, SD = 0.08 m a^{-1}) and Langshisha (mean = −0.09, SD = 0.07 m a^{-1}) during this period. Surface elevation and volume change were constrained to the ablation zone for the period (LIA-2000 CE).

4.1.3. Overall glacier changes since the LIA

4.1.3.1. Area changes from LIA to 2023. Between the LIA (1815 CE) and 2023 CE, the Langtang Catchment lost 78.46 ± 4.38 km^2 (~41.25 ± 1.62%) of glacier area at the rate of 0.2 ± 0.01% a^{-1} or 0.38 $km^2\ a^{-1}$ (Table 1). Over this period, the number of glaciers nearly doubled from 58 to 115, mainly due to separations of tributary glaciers from the compound valley glaciers and lateral fragmentations of clean-ice glaciers. All glaciers mapped in 2023 had receded relative to their LIA position (Fig. 5a & Figs. 6a-j), and eight clean-ice glaciers (~2.48 km^2;

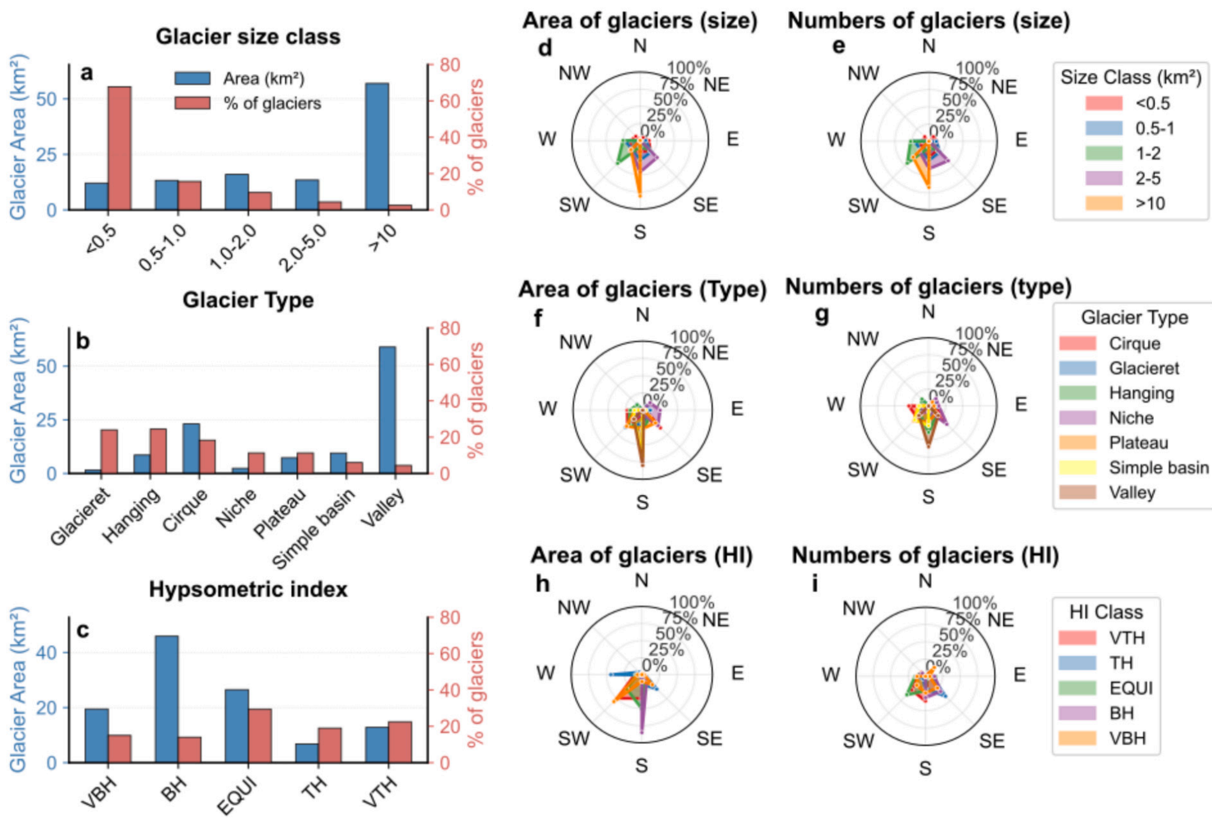

Fig. 2. Glacier characteristics in the Langtang Catchment (2023). (a) Glacier size-class distribution by area and percentage. (b) Glacier-type distribution by area and percentage. (c) Glacier-HI distribution by area and percentage. (d–e) Aspect distribution of glacier area (%) and number (%) by size class. (f–g) Aspect distribution of glacier area (%) and number (%) by type class. (h -i) Aspect distribution of glacier area (%) and number (%) by HI.

three between LIA –1964; one 1964–1974; four between 1974 and 2016) completely disappeared. This widespread area shrinkage also changed the glaciers' hypsometric distribution within the catchment. Notably, all glacier area below 4000 m a.s.l. has been lost, with most significant area loss concentrated at the median elevation range ~ 5000–5800 m asl (Fig. 5b).

4.1.3.2. Area changes from LIA to 1964 and 1964–2023. From the LIA to 1964, the Langtang Catchment lost 32.14 ± 4.64 km^2 (~16.90 ± 2.35%) of glacier area, shrinking at the rate of 0.11 ± 0.016% a^{-1} or 0.22 km^2 a^{-1} (Table 1). During this period, all glaciers receded, and the number of glaciers increased from 58 to 75, mainly driven by separation of tributary glaciers from the main trunk of valley glaciers. Between 1964 and 1974, the catchment further lost 7.0 ± 4.14 km^2 (4.43 ± 2.6%) of glacier area at the rate of 0.7 km^2 a^{-1} (0.44 ± 0.26% a^{-1}), ~four times the rate of area loss between the LIA and 1964. During this decade, the glacier number increased from 75 to 83, both from tributary separation and lateral fragmentation.

Glacier shrinkage continued from 1974 to 2000 at marginally higher rate. Utilizing corrected RGI v7.0 outlines, we computed an area loss of ~18.37 ± 4.6 km^2 (–12.16 ± 3%) corresponding to annual rate of 0.71 km^2 a^{-1} (0.47 ± 0.12% a^{-1}). During this period, glacier numbers increased from 83 to 100, due to increased fragmentation in glaciers such as GL1, GL2, Lirung, and Yala (Fig. 5), which experienced some of the highest area loss rates (ranging from 1.03% a^{-1} to 1.81% a^{-1}). The most rapid shrinkage was observed between 2000 and 2016, where the catchment lost 16.87 ± 3.52 km^2 (12.71 ± 2.7%) at the highest rate of 1.05 km^2 a^{-1} (0.79% a^{-1}). In the most recent period (2016 to 2023), the catchment further lost 4.08 ± 2.40 km^2 at the rate of 0.58 km^2 a^{-1} (0.50 ± 0.3% a^{-1}). Despite the shorter observation window (7 years), the difference in this rate of area loss was significant (*t-value* = −2.06, p = 0.04) when compared with the rate of change from 2000 to 2016 using a paired-test.

From 2000 to 2023, the catchment lost ~20.95 ± 3.9 km^2 (15.8 ± 2.9%) of glacier area at the rate of 0.91 km^2 a^{-1} (0.69 ± 0.13% a^{-1}), ~1.5 times faster than the retreat rate observed between 1964 and 2000. Over the satellite era (1964 to 2023), the catchment altogether lost 46.32 ± 3.4 km^2 of glacier area at the rate of (0.49 ± 0.01% a^{-1} or 0.76 km^2 a^{-1}).

Across the whole satellite era (1964 to 2023 CE), debris-covered glaciers also shrank, by ~10% at the rate of 0.57% a^{-1}, mainly due to the terminus retreat (Supplementary Figs. S7a–c & Table S7). However, supraglacial debris cover increased by ~7.3%, from 28.92 ± 0.98 km^2 to 31.03 ± 0.87 km^2, driven by debris emergence at the termini of two formerly clean-ice glaciers (Yala & GL3) and upslope expansion of debris-cover on existing debris-covered glaciers due to enhanced mass wastage from deglaciated surfaces (Supplementary Figs. S7a–c). Overall, clean-ice glaciers receded faster than the debris-covered glaciers in the catchment (Figs. 6g-h).

Large valley glaciers and simple basin type glaciers each lost ~35% of their LIA area at the rate of 0.1% a^{-1} and 0.16% a^{-1} between LIA and 2023 CE, respectively, mainly from the tributary glacier separation (Figs. 6c-d). Plateau type glaciers lost more than ~50% of their total LIA area at the rate of 0.14% a^{-1} (Figs. 6c-d), due to extensive recession and lateral fragmentation. Among plateau type glaciers, Yala Glacier has only 24% area remaining of its LIA extent (~6.41 km^2 in LIA and ~ 1.54 km^2 in 2023) and is one of the fastest receding glaciers (at the rate of 0.18% a^{-1} from LIA to 2023 CE) in the catchment.

While larger glaciers lost more area in absolute terms ($r = -0.92$, $p < 0.001$), smaller glaciers showed a significantly faster relative loss rate ($r = 0.28$, $p = 0.046$) (Figs. 6a-b). In terms of hypsometric index, VTH, TH, and EQUI glaciers showed higher area loss rates than VBH and BH

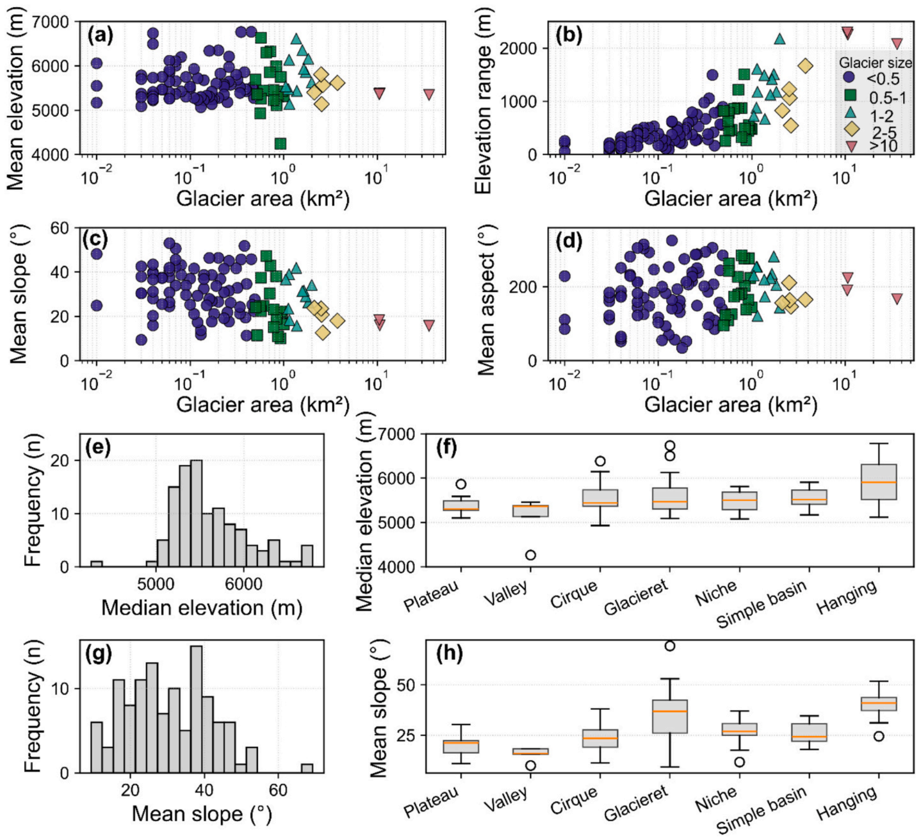

Fig. 3. Topographic characteristics of glaciers in 2023. Scatter plots of glacier size versus glacier mean elevation(a), elevation range (b) average slope (c), and average aspect (d), respectively, for different galcier size class. Histogram of glacier median elevation (e). Box plots of glacier median elevation for different glacier types (f). Histogram of glacier median slope (g). Box plots of mean glacier slope for different glacier types (h). Glacier area and inventory derived from Sentinel imagery of 2023 and void filled 30 m SRTM.

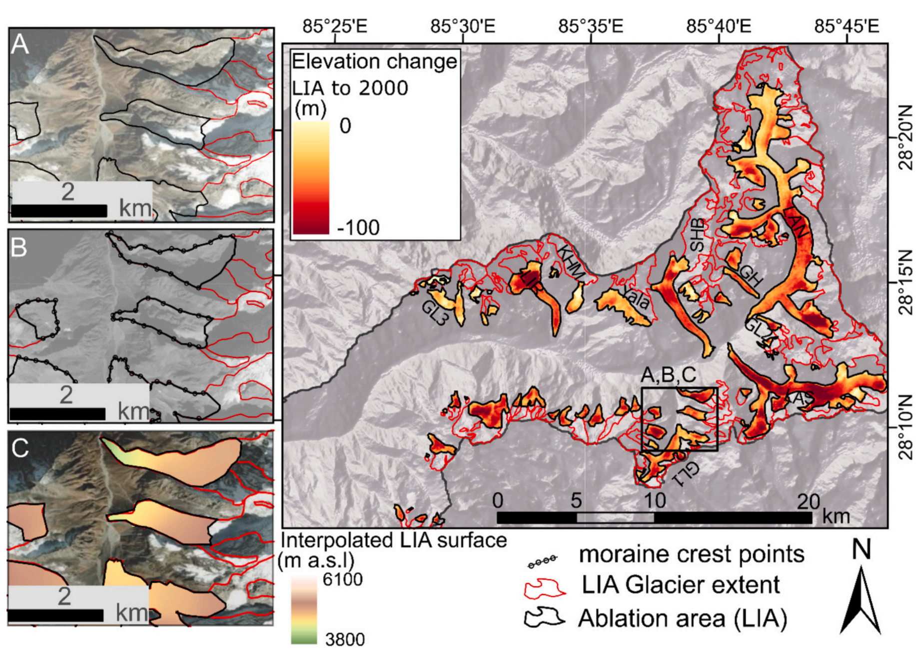

Fig. 4. Reconstruction of LIA glacier extent, glacier surface and elevation change in Langtang Catchment. (A) LIA maximum extent mapped from moraine crestlines and trimlines by extending glacier outlines from RGI v.7.0. on Sentinel imagery (B) reconstruction of LIA glacier surfaces using SRTM DEM from 2000 (C) Interpolated surface area for ablation areas, and (D) surface elevation change derived from differencing reconstructed glacier surface with SRTM DEM from 2000. Glacier labels: LIR (Lirung), KHM (Khimsung), GH (Ghanna), LAN (Langtang), LAS (Langshisha). GL1–GL3 denote unnamed glaciers.

(Fig. 6e-f), largely because these classes contained smaller size glaciers. However, statistical differences in area change rates among

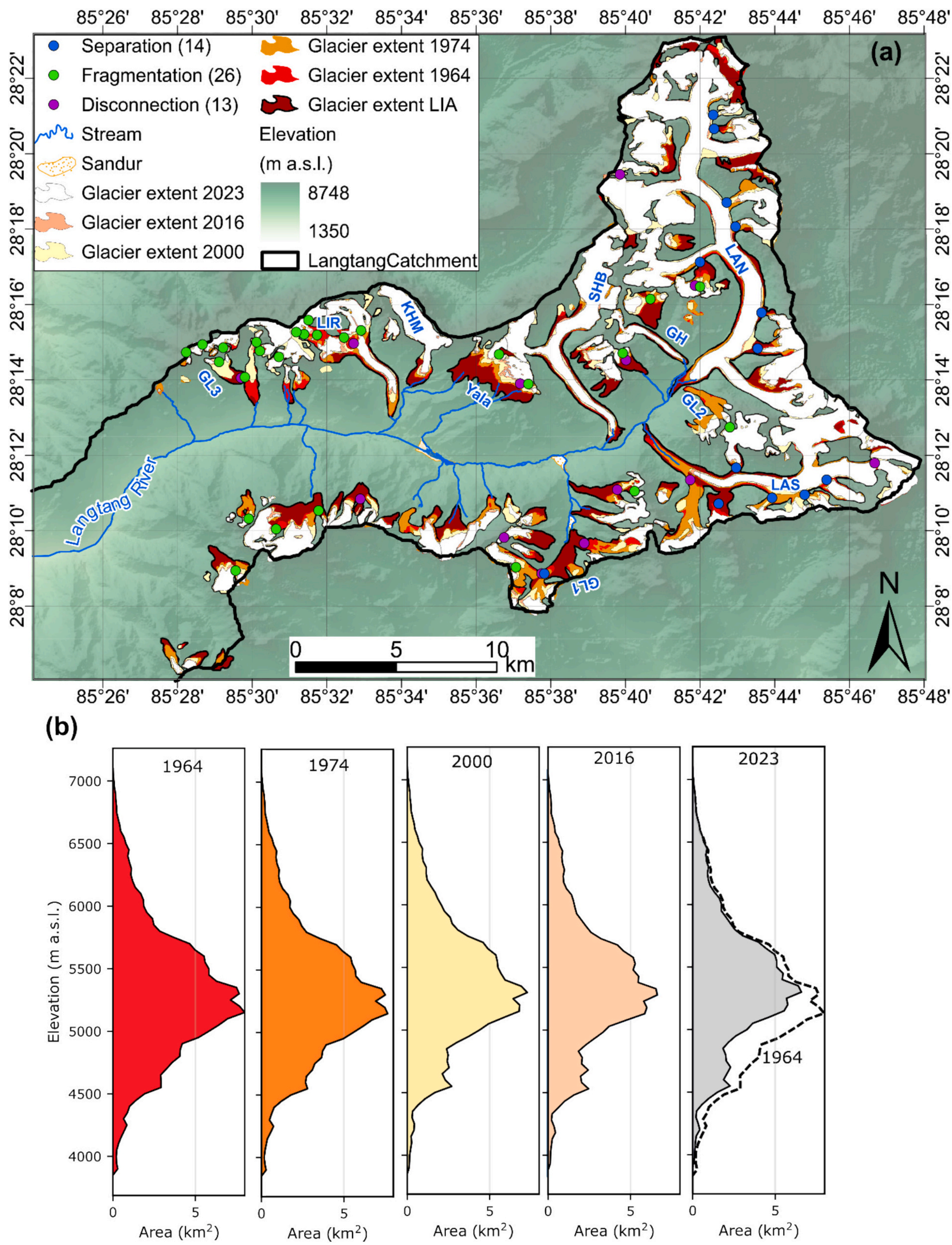

Fig. 5. Spatio-temporal glacier changes in the Langtang Catchment. (a) Glacier extents in different years with glacier disconnection (pink dot), fragmentation (green dot), and separation (blue dot) shown for year 2023. Glacier labels: LIR (Lirung), KHM (Khimsung), GH (Ghanna), LAN (Langtang), LAS (Langshisha); GL1–GL3 denote unnamed glaciers.GL1, GL2, and GL3 are glaciers with no names and labelled as 1, 2, and 3; (b). Hypsometric distribution of glacier area for each mapped year. Curves were derived by intersecting the 1-arcsecond SRTM DEM (c. 2000 CE) with the respective annual glacier outlines. Note: The 2000 CE SRTM DEM was utilized as a static topographic reference for all periods due to data availability. (For interpretation of the references to colour in this figure legend, the reader is referred to the web version of this article.)

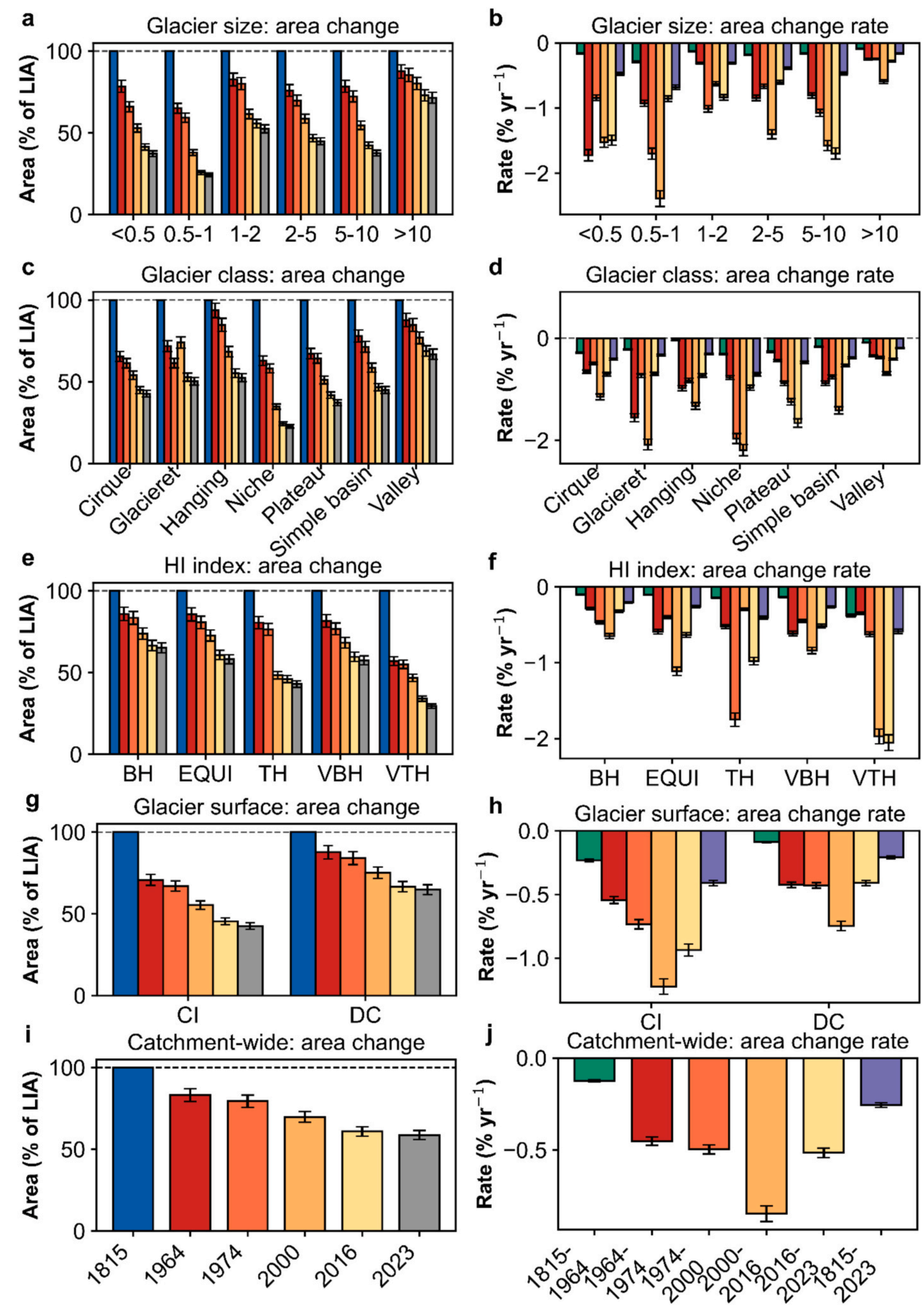

Fig. 6. Glacier area change in the Langtang catchment expressed as relative area change (%) remaining to LIA and area change rate (% a^{-1}) for each period. Panels (a–b) show changes by glacier size class; (c–d) by glacier morphological type; (e–f) by hypsometric index; (g–h) by debris cover (clean-ice-CI vs. debris-covered-DC); and (i–j) for catchment-wide glacier change. Bars are colour coded as per the period/year.

Hypsometric Index (HI) classes were not significant.

Further, linear regression analysis (Figs. S9a-d) showed small glaciers (<1 km^2) with mean elevation ~5200 m a.s.l. experienced significantly higher relative rates of area loss (−1.1 to −1.8% a^{-1}) compared to the larger glaciers (>5 km^2; <−0.25 to −0.5% a^{-1}) with similar mean elevation. Additionally, glaciers with predominantly S–SE aspects and mean slopes of 25–35°, common in the catchment showed higher area loss rates (1.5 to 1.8% a^{-1}), however, these relationships were not statistically significant.

4.1.3.3. Glacier disconnection, fragmentation, and separation. In addition to mapping glacier extent for different years, we quantified glacier disconnections, fragmentations, and separations across all observation periods to assess their temporal evolution (Supplementary Table S8). In 1964, five tributary separations (two in Langtang, three in Langshisha) and nine fragmentations were mapped, indicating that glaciers in the catchment were retreating and shrinking substantially prior to 1964. By 1974, four additional fragmentations on Lirung and Langshisha glaciers were mapped, while no further separations occurred. Sentinel 2 A imagery from 2016 revealed significant glacier changes, with 11 glacier disconnections, 22 fragmentations, and 14 separations. In 2023, we mapped 26 glacier fragmentations, 13 disconnections, and 14 separations (Fig. 5a), highlighting the continued glacier recession in the catchment.

Lirung Glacier in 2023 had six smaller clean-ice units in its accumulation areas, whereas the debris-covered tongue disconnected from its accumulation between 1974 and 2000. Similarly, Langshisha Glacier exhibited two distinct flow units, with five separated tributary glaciers in 2023. The Langtang Glacier, underwent seven tributary separations whereas a plateau-type Yala Glacier underwent both along-flow disconnection and lateral fragmentation forming three distinct fragments as of 2023 (Fig. 5a). GL1, a valley glacier with three tributaries and an area of 8.21 km^2 during the LIA, fragmented into five smaller ice masses totalling ~2.11 km^2 by 2023, retaining only ~26% of its LIA area.

Our results further showed that separations primarily mapped on the valley floors of the large compound valley glaciers occurred at relatively lower elevations (mean = 5080 m a.s.l., SD = 134) and on average slopes of ~23°. In contrast, disconnections occurred at slightly higher elevations (mean = 5135 m a.s.l., SD = 274) and on steeper slopes (~34°) and were generally associated with the steep, highly crevassed, and thinned ice icefall regions. Disconnection led to along-flow severance within a glacier polygon. Fragmentations were predominantly mapped on smaller glaciers located at higher elevations (mean = 5200 m a.s.l., SD = 190) and on the steepest slopes (~35°), where glacier thinning rates were also elevated (Supplementary Figs. S10b–c).

4.2. Glacier and climate change in the recent period (1960–2023)

4.2.1. Mass balance (MB) and equilibrium line altitude (ELA) change

Reconstructed catchment-wide mass balance (MB) using OGGM was positive or in a balanced state during the 1960s and 70s (0.50 ± 0.09 m w.e. a^{-1}) but became persistently negative (−0.19 ± 0.01 m w.e. a^{-1}) after the 1980s. The most negative MB occurred in 2000–2010 (−0.52 ± 0.06 m w.e. a^{-1}) and 2011–2017 (−0.51 ± 0.18 m w.e. a^{-1}) (Fig. 7a).

Individual glacier MB time series showed a coherent MB pattern (Fig. 7c & Supplementary. Figs. S11a-f), likely due to the use of coarse resolution climate forcing inputs. However, their mass loss magnitudes varied with high inter-annual variability, largely due to their size, geometry, and elevation range. For example, small glaciers like Lirung Glacier exhibited the most pronounced cumulative loss (~38 m w.e. since 1990), followed by Yala (~15 m w.e.), Langshisha (~14 m w.e.), and Langtang (~5 m w.e.) (Fig. 7c). In contrast, large debris-covered glaciers (e.g. Langtang and Shalbachum) showed relatively smaller cumulative losses, likely due to the presence of thick debris layers, extensive elevation range, and high-elevation accumulation areas.

Alongside, the simulated regional ELA of the catchment rose steadily from the 1960s (Fig. 7b), consistent with the increasing negative MB. The catchment's mean ELA increased from 5360 ± 122.6 m a.s.l. in 1960–1970 to 5532 ± 110 m a.s.l. in 2000–2020 (a total rise of ~175 m) (Supplementary Table S9). This ~175 m ELA rise resulted in a noticeable reduction in the accumulation area in the catchment. For many smaller, lower-elevation glaciers, the current ELA now lies consistently above their upper glacier boundaries, indicating a near-permanent mass-balance disequilibrium and ongoing mass loss driven by ablation. For example, Yala Glacier, which is located at relatively low elevation, shows the largest ELA increase (~+200–250 m since the 1980s). Its ELA is now above 5600 m a.s.l., higher than the glacier's maximum extent, meaning the entire glacier is now in the ablation zone.

4.2.2. Surface elevation changes

Glacier surface elevation changes in the Langtang Catchment for the period (2000–2019) assessed with spatiotemporally resolved datasets of Hugonnet et al. (2021) showed a clear overall increase in glacier thinning rates over the period (Figs. 8a–d & Supplementary Table S10a). The mean glacier-wide thinning rate for the catchment increased from −0.41 ± 0.14 m a^{-1} (2000–2004) to −0.77 ± 0.11 m a^{-1} (2015–2019). Thinning also expanded to higher elevations, including icefall regions, at the transition zone between debris-covered mantle and clean-ice in the debris-covered glacier, and accumulation areas during this period. In these regions, the average thinning rate increased from −0.38 ± 0.12 m a^{-1} to −0.50 ± 0.12 m a^{-1}, with icefalls of Shalbachum, Langshisha, and Langtang glaciers experiencing high thinning rates > −2.5 m a^{-1} (Figs. 8a-d). Debris-covered glaciers showed the highest thinning in their mid-sections, extending up to the maximum extent of the debris cover (e.g. ~4600–5400 m a.s.l. for Langtang Glacier; ~4800–5000 m a.s.l. for Shalbachum, and ~ 5000–5200 m a.s.l for Langshisha Glacier; Supplementary Figs. S12a-f). Notably, Khimsung Glacier, which showed mass gain in its broad accumulation area during 2000–2009 (Figs. 8a–b), experienced substantial thinning during the subsequent periods of 2010–2014 and 2015–2019 (Figs. 8c–d). Note that the uncertainty expressed here is median absolute deviation (MAD).

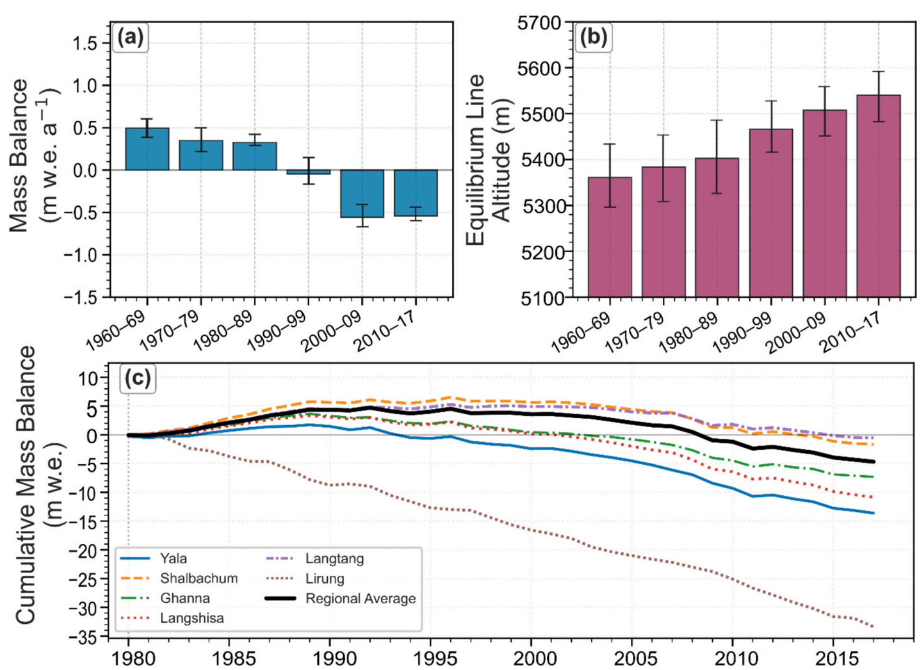

Fig. 7. Decadal variability of (a) regional glacier mass balance (MB) and (b) equilibrium-line altitude (ELA) in the Langtang Catchment from 1960 to 2020, simulated by OGGM. Values represent catchment-wide, area-weighted averages of individual glacier MB and ELA aggregated by decade. Boxes show the interquartile range (25th–75th percentiles). (c) Cumulative mass balance of major glaciers in the catchment since the 1980s.

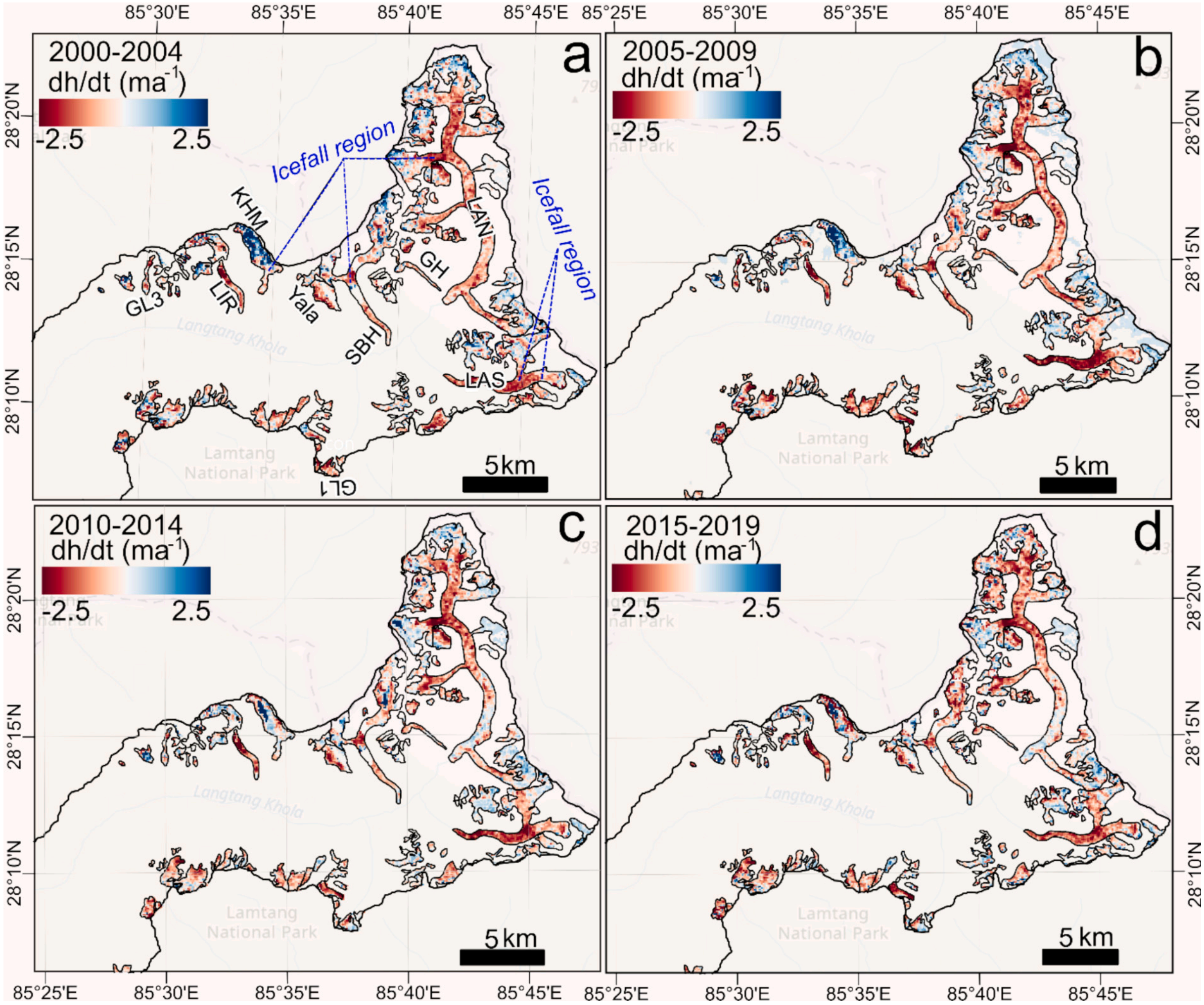

Fig. 8. Spatial patterns of mean glacier surface elevation change rate in the Langtang Catchment over the period 2000 to 2019 (a–d). Glacier labels: LIR (Lirung), KHM (Khimsung), GH (Ghanna), LAN (Langtang), LAS (Langshisha). GL1, GL2, and GL3 do not have local names.

Major glaciers such as Langtang, Langshisha, Shalbachum, Lirung, and Yala, all experienced increased thinning, with thinning more pronounced in their ablation zones in all periods (Figs. 8a-d & Supplementary Table S10b). Langtang and Shalbachum also showed some elevation gain at their terminus part. This thickening could likely be due to advection of ice and debris englacially and through supraglacial channels, leading to localized increase in surface elevation to near stationary terminus (Scherler et al., 2011; Pellicciotti et al., 2015), though the specific drivers causing this requires further investigations. These elevation changes resulted in a total glacier volume loss of 0.29 km^3 (-0.059 km^3 a^{-1}) during 2000–2004 and 0.45 km^3 (-0.09 km^3 a^{-1}) during 2015–2019 (Supplementary Table S10a), indicating that the loss rate increased by about 1.5 times in the later period. The corresponding mean geodetic mass balance became more negative, decreasing from -0.35 ± 0.45 m w.e. a^{-1} (2000–2004) to -0.53 ± 0.44 m w.e. a^{-1} (2015–2019). Over the full 2000–2019 period, the average geodetic mass balance was -0.44 ± 0.32 m w.e. a^{-1}. All estimates for volume and volume-to-mass change used the glacier area from 2000 CE, derived from corrected RGI v7.0 glacier extents and an assumed ice density of 850 kg m^{-3}. The reported uncertainty in geodetic mass balance represents ±1 standard deviation (±1σ).

4.2.3. *Glacier surface velocity change*

Temporal analysis of annual surface velocities (ITS_LIVE;1988–2022) showed a widespread slowdown in glacier surface velocity in the catchment (Figs. 9a–e), irrespective of their surface characteristics. In the late 1980s, most glaciers exhibited active flow across their ablation zones, with average annual velocities ranging from 11 to 60 m a^{-1} (Fig. 9a). By contrast, between 2016 and 2022, there was a widespread decrease in glacier surface velocities, especially over debris-covered tongues, where mean annual surface velocities declined to <5 m a^{-1}, indicating rapid decline and near-stagnant flow (Figs. 9a-e).

The average annual catchment-wide velocity with median absolute deviation (±MAD) decreased from 5.2 ± 2.1 m a^{-1} in 1988 to 2.8 ± 2.2 m a^{-1} in 2022. This corresponded to 17% dec^{-1} (Supplementary Fig. S14). After 2003, catchment-wide average velocities remained consistently ≤5 m a^{-1}, with a low interannual variability, in contrast to higher interannual variability between 1988 and 2000 (Supplementary Fig. S14). However, glacier-wide mean velocities varied by glacier types (Supplementary Figs. S14-S15). Clean-ice glaciers showed mixed flow dynamics. For example, Khimsung Glacier, a top-heavy glacier, showed increasing median flow velocities from 11.34 ± 2.45 m a^{-1} (1988) to 21.83 ± 3.25 m a^{-1} (2022), an increase of ~45%. Conversely, Yala Glacier, a plateau type glacier, displayed a steady decline from 5.07 ± 1.65 m a^{-1} to 3.59 ± 1.25 m a^{-1}, a slowdown by ~29% in their annual flow velocities, over the same period.

Debris-covered glaciers on the other hand showed consistent decreases in surface velocities, with ablation zone's velocity typically below 10 m a^{-1} in most recent years (Figs. 9a-e). Langtang Glacier, the

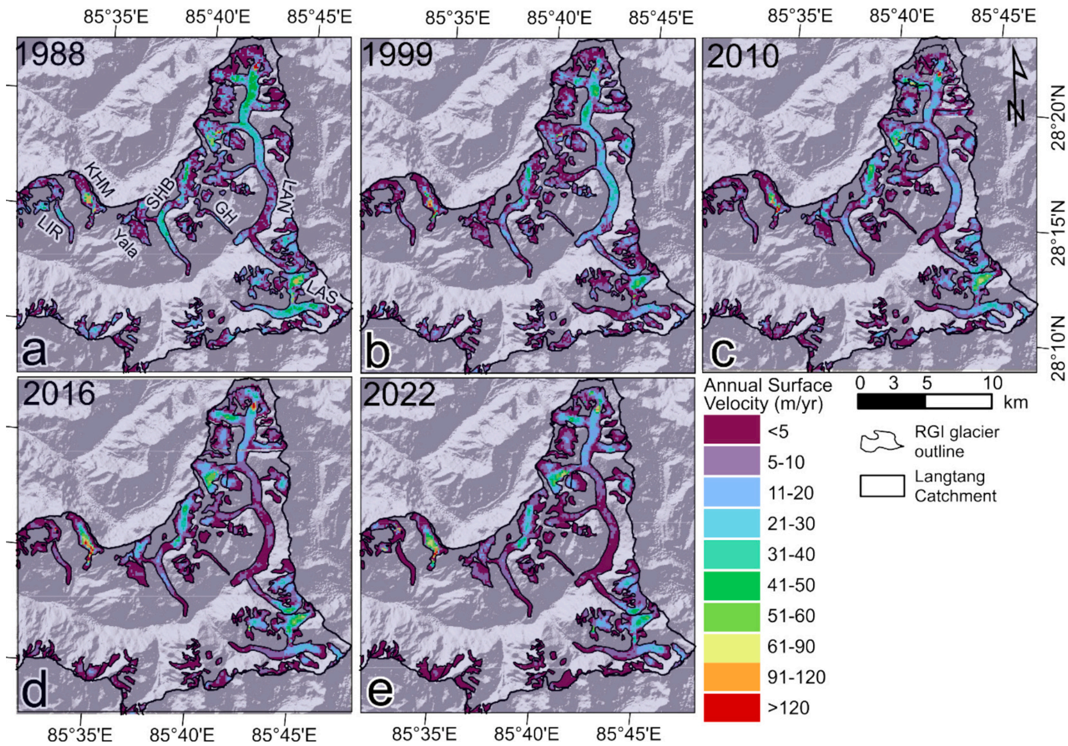

Fig. 9. Multi-temporal glacier surface velocity (m a^{-1}) in the Langtang Catchment derived from ITS_LIVE velocity fields between 1988 and 2022. Panels (a–e) show glacier-wide mean annual ITS_LIVE velocity field from 1988, 1999, 2010, 2016, and 2022. Glacier labels: LIR (Lirung), KHM (Khimsung), GH (Ghanna), LAN (Langtang), LAS (Langshisha).

largest glacier, also showed significant velocity reductions in its lower reaches over the period, whereas the Lirung, Langshisha, and Ghanna glaciers have remained nearly stagnant (<10 m a^{-1}) since 2003 (Supplementary Figs. S14-S15). Based on the threshold of 10 m a^{-1} (Pellicciotti et al., 2015), as of 2022, the stagnant portion of the debris covered tongues for Langtang was ~8.4 km, Langshisha, ~4.2 km, Shalbachum, ~2.6 km, Ghanna, ~ 3.2 km; and Lirung, ~3.5 km.

The highest velocities >100 m a^{-1} occurred in the steep icefall areas of Khimsung Glacier and in the transition zone between clean-ice and debris-covered ice on Langtang Glacier throughout the period (Figs. 9a–e). However, velocity estimates in these regions may be affected by "surface skipping" or "locking" artifacts in ITS_LIVE data and should therefore be interpreted with caution (Dehecq et al., 2019). Despite these localized areas of high velocities, glacier-wide average surface velocities have steadily declined in these glaciers since 1988, except for Khimsung Glacier, where velocities increased (Supplementary Figs. S14-S15), likely due to the sustained and continued ice flux from its wide and extensive accumulation area and presence of steep, heavily crevassed icefall regions on the glacier that facilitates meltwater delivery to the glacier bed, enhancing basal sliding and ice motion.

The anomalously high velocities in 2002 and 2003, resulting from limited measurement points (verified using pair-count metadata from the ITS_LIVE dataset), were excluded from the analysis. We further acknowledge that the ~200 m spatial resolution of ITS_LIVE data might also have underestimated velocities in narrow glacier tongues (~340–1000 m wide) due to spatial averaging and smoothing (Pronk et al., 2021). Nevertheless, this dataset is useful for assessing long-term basin- and glacier-scale trends, and velocities for narrow valley glaciers are interpreted as conservative estimates.

4.2.4. *Temperature and precipitation trends (1960–2023)*

The Langtang Catchment has experienced significant climate warming since 1960, characterized by pronounced elevation dependence (Fig. 10a) and strong seasonality (Supplementary Fig. S16a & Table S11). Glacierized areas (>4000 m a.s.l) warmed at 0.31 °C dec^{-1} ($p < 0.05$), more than three times the rate observed at the lower elevation- Kyangjin AWS (~3865 m a.s.l; 0.10 °C dec^{-1}, $p = 0.023$). Observations from the Kyangjing station (Fig. 10a) corroborated this trend, showing a warming trend of 0.42 °C dec^{-1} between 1988 and 2012 ($p > 0.05$). These warming rates are slightly higher than 0.28 °C dec^{-1} observed for the Hindu Kush Himalaya (HKH) (Jackson et al., 2023) and much higher than the global mean warming rate of 0.06–0.07 °C dec^{-1} for 1980–2020 (Forster et al., 2024). This enhanced warming in the glacierized areas in the catchment likely reflects the combined influence of snow- and ice-albedo feedbacks, changes in atmospheric moisture and cloudiness, and enhanced long-wave radiative forcing in high-mountain environments (Mountain Research Initiative EDW Working Group, 2015), however, needs a detailed investigation.

The warming trend increased substantially in recent decades relative to the baseline period (1960–1990). Mean temperature anomalies over the glacierized areas (>4000 m a.sl) increased from ~1.13 °C between 2000 and 2010, to ~1.35 °C between 2010 and 2020, and to ~1.67 °C between 2015 and 2023 compared to ~ − 0.0018 °C between 1960 and 1990. Seasonally, substantial warming was observed in the autumn (September, October, and November) with an average increase of ~0.55 °C, followed by winter (December, January, and February) at 0.51 °C. Spring (March, April, and May) and summer (June, July, and August) seasons also experienced positive temperature anomalies of 0.46 °C and 0.45 °C, respectively, indicating year-round warming over the glacierized area in the catchment (Supplementary Fig. S16a & Table S11).

No significant long-term trend was detected in annual precipitation for both ERA5-Land (1960 to 2023) and observed precipitation from Kyangjing station (1980 to 2014; Fig. 10b). However, seasonal anomalies showed a decline in summer precipitation by −0.63% and autumn by −2.99%, respectively, while winter and spring experienced increases of 5.4% and 6.36%, respectively (Supplementary Fig. S16b & Table S11).

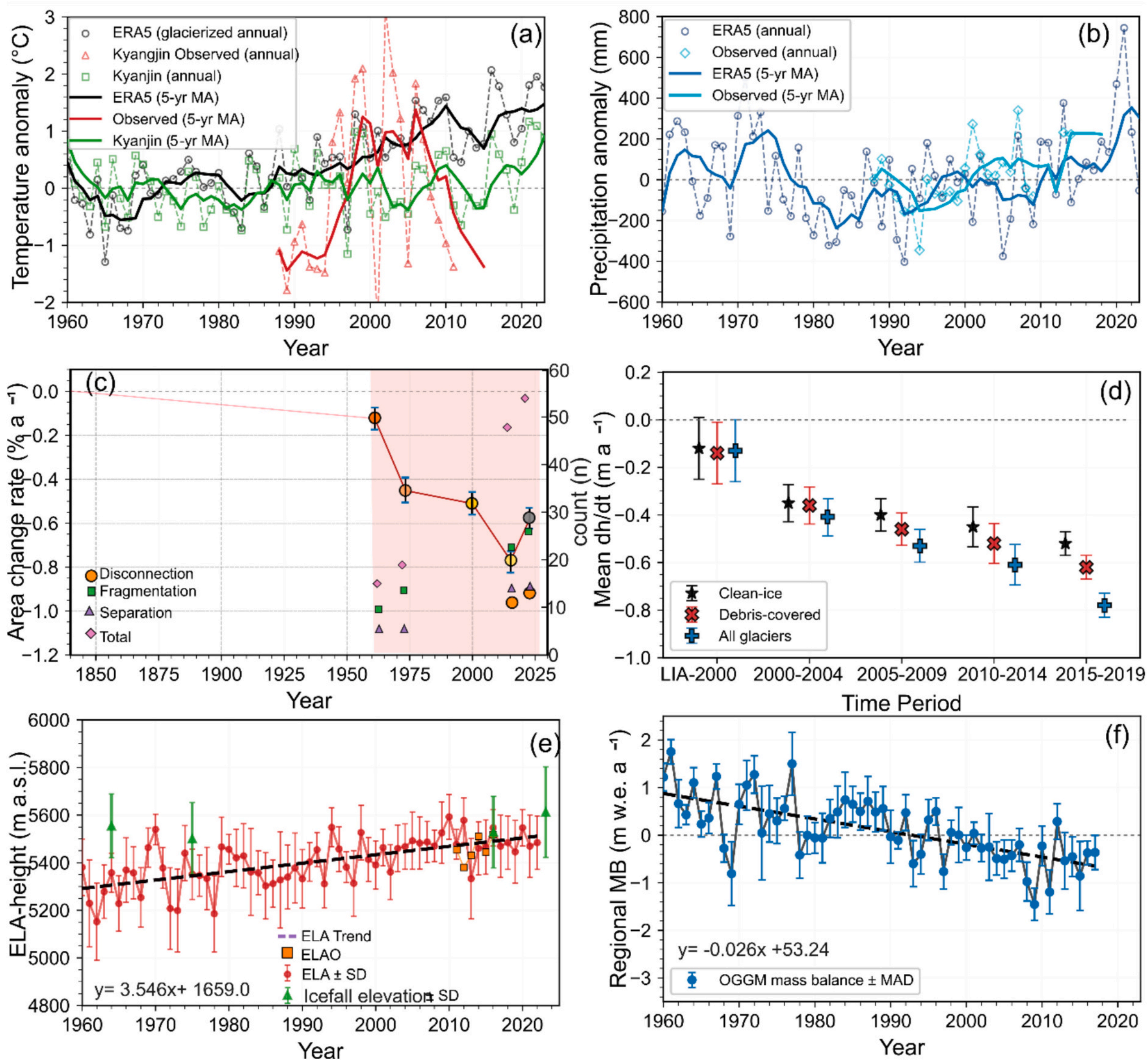

Fig. 10. Summary plots of climate and glacier change in the Langtang Catchment. (a) Mean annual 2 m ERA5- Land temperature anomaly for all glacierized areas (black circle), observed anomalies at Kyanjing AWS (~3865 m a.s.l; red triangle), and ERA5-Land anomalies at the Kyanjing grid point (green square). (b) Mean ERA5-Land annual precipitation anomalies (blue circle) and observed anomalies (sky-blue diamond). ERA5-land anomalies calculated over 1960–2023 relative to 1960–1990; observed anomalies from Kyangjing station (1986–2015). Trend lines are 5-year moving averages. (c) Glacier area change rates since LIA (~1815 CE) to 2023 and numbers of disconnection, fragmentation, and separation per mapping period. (d) Glacier area-averaged thinning (dh/dt) by glacier types. (e) Regional ELA simulated with OGGM, with observed ELA for Yala Glacier (2011–2017, orange square) and median icefall elevations (green triangle) with standard deviation (SD). (f) Light pink shading in Fig. (c) indicates the glacier mapping periods. (For interpretation of the references to colour in this figure legend, the reader is referred to the web version of this article.)

5. Discussion

5.1. *Overall changes in glacier area, rates of change, and comparison with regional glacier change studies*

Our assessment of glacier area changes in the Langtang Catchment from the LIA (~1815 CE) to 2023 CE revealed sustained glacier shrinkage, with significant acceleration during the satellite era (Fig. 10c). While long-term area loss rate was relatively modest (~0.11% a^{-1}) during LIA-1964, it increased more than fourfold (~0.49% a^{-1}) during 1964–2023, concomitant with the enhanced warming at higher elevations and increasing thinning and mass loss in the catchment (Figs. 10a, d, f). The most rapid area loss occurred between 2000 and 2016 (~0.79% a^{-1}). Although the rate declined slightly during the most recent period (2016–2023; ~0.51% a^{-1}), likely due to the shorter observation window, it remained statistically significant and higher than during the early satellite era (1964–1974; ~0.44% a^{-1}). Overall, the accelerated glacier area loss is consistent with increasing warming rates (Section 4.2.4; Fig. 10a) and sustained negative mass balance in the Langtang Catchment (Fig. 10f).

It is noteworthy that our glacier area loss rate for extended timescales (LIA–1964/2023) are subject to uncertainty due to the poorly constrained LIA maximum timing and the lack of historical glacier outlines before the satellite era. While we adopted 1815 CE as the reference LIA timing following Kayastha and Harrison (2008), some studies suggested that the LIA maximum timing was asynchronous, potentially persisting until 1910 CE. A sensitivity test for long-term rates, using a broader range of LIA maximum dates reported for the Himalaya and for a few glaciers in the Langtang Catchment (~1300 CE to ~1910 CE; e.g. Shiraiwa and Watanabe, 1991; Barnard et al., 2006; Rowan, 2017; Qureshi et al., 2021) reveals that long-term area change rates vary significantly from 0.02 to 0.32% a^{-1} (LIA:1300–1910 –1964) and 0.06 to 0.36 (LIA:1300–1910–2023) compared to estimates of ~0.11% a^{-1} (1815–1964) and ~ 0.20% a^{-1} (1815–2023) (Table 1).

Regardless of the sensitivities to LIA timing, the Langtang catchment clearly had experienced strong glacier shrinkage post LIA. Depending upon the selected LIA maximum timing, area loss rates in recent decades were ~ 1.5 to 20 times higher than the long-term historical average and accelerated in recent decades (Fig. 10c) and driven by contemporary climatic warming in the catchment (Fig. 10a).

Furthermore, our estimates of annualized catchment-wide glacier area loss rates during the satellite period (0.49% a^{-1}; 1964–2023) and the most recent period (0.50% a^{-1}; 2016–2023) fit in well with the area loss rates reported across Nepal and the greater Himalayan region (Fig. 11). These rates are however, lower than the Nepal-wide area loss rate (~0.78% a^{-1} for 1980–2010; Bajracharya et al., 2014) and higher than those documented for the Khumbu region (0.12–0.40% a^{-1} for 1962–2007 and 1964–2011; Bolch et al., 2008; Thakuri et al., 2014) and parts of the western Indian Himalaya (~0.2–0.4% a^{-1} over various periods) but still fall within the broader range of reported Himalayan glacier area-loss rates (approximately ~0.1 to ~0.8% a^{-1} across different regions and time periods). In contrast, the rates closely match rates observed in the Kanchenjunga region (0.5% a^{-1} for 1962–2006; Racoviteanu et al., 2015) and Everest south (0.52% a^{-1} for 1962–2006; Nie et al., 2010). These regional discrepancies likely reflect differences in data sources, mapping methodologies, observation periods, and the influence of local climatology, topography, and glaciological factors such as mass balance and ice thickness (Brun et al., 2019; Fujita and Nuimura, 2011; Maurer et al., 2019; Scherler et al., 2011).

5.2. Glacier surface mass balance and ELA changes

While glacier area changes translate into a delayed signal of climate change (Oerlemans, 2001; Bolch et al., 2011), glacier MB provides a direct measure of glacier-climate interactions and is central to understanding the drivers of glacier change (Gardelle et al., 2013; Stumm et al., 2021; Fujita et al., 2006). Our catchment-wide MB reconstructions show that glaciers in the Langtang catchment transitioned from near-balanced state in the mid-20th century to accelerating mass loss after 1990s (Fig. 7a & Fig. 10f). This coincides with significant warming of 0.3 °C dec^{-1} or 0.03 °C a^{-1} over 1960–2023 across the glacierized areas in the catchment (Fig. 10a). Increasingly negative mass balance after the 1990s is evident in cumulative mass balance for major glaciers (see Fig. 7c), corresponding to higher temperature anomalies of 1.13 °C during 2000–2010 and 1.35 °C during 2010–2020 (Supplementary Table S9). As glaciers in the catchment are summer-accumulation type, their MB is strongly controlled by summer temperature and snow accumulation. While precipitation has high interannual variability without a significant long-term trend (Fig. 10b), enhanced warming at higher altitudes appears to be the primary driver of mass loss in the catchment, consistent with broader central Himalayan observations where increasing precipitation totals have not been able to offset temperature-driven glacier mass loss (Bhattacharya et al., 2021; Kraaijenbrink et al., 2017).

OGGM-simulated MB for the past two decades after 2000 (−0.52 ± 0.06 m w.e. a^{-1} for 2000–2009 and − 0.51 ± 0.18 m w.e. a^{-1} for 2010–2017) are in line with the geodetic MB estimates for Langtang sub-region (−0.58 ± 0.13 m w.e. a^{-1} for 2016–2019; Bhattacharya et al., 2021; Supplementary Figs. 11a-f). The simulated positive or near-balanced MB before 1990s (Fig. 10f) is however, inconsistent with observed glacier area loss during this period and is more positive than geodetic MB estimates (−0.20 ± 0.09 m w.e. a^{-1} for 1964–1974; Bhattacharya et al., 2021). This discrepancy arises because OGGM's automated calibration before 2000 relied on interpolated mass balance data from the nearest World Glacier Monitoring Service (WGMS) reference glaciers, which were located outside the catchment. Therefore, the simulated MB by OGGM before 2000 should be interpreted carefully. In contrast, the good agreement between simulated and geodetic MB after 2000 (Supplementary Figs. 11a–f), as well as with observed glacier area loss rates (Fig. 10c), reflects the improved calibration using glacier-specific geodetic MB from Hugonnet et al. (2021) for individual glaciers.

The regional ELA of the catchment which qualitatively indicates the variation in the SMB (Chinn et al., 2005), has risen steadily over the period (Fig. 7b & Fig. 10e), potentially driven by declining snow cover area and snow persistence (Pradhananga et al., 2025; Muhammad and Thapa, 2021) and sustained negative MB (Fig. 10f). As the catchment is experiencing amplified warming at higher elevations, an increasing proportion of precipitation likely fall as rain rather than snow. The

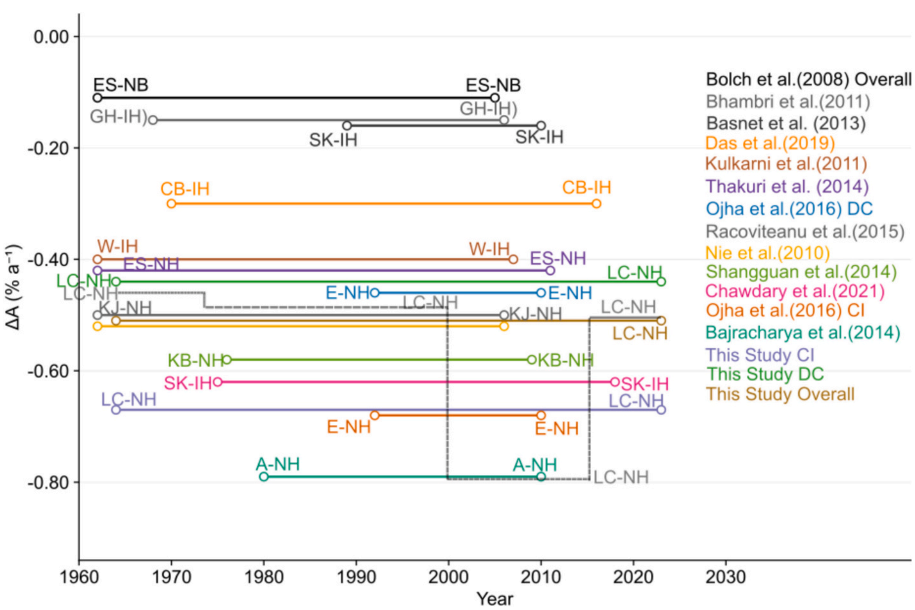

Fig. 11. Comparison of glacier area change rates derived in this study with estimates reported across the Himalayan region. Regional abbreviations are as follows: All (A), Everest South (ES), Sikkim (SK), Kanchenjunga (KJ), Eastern Himalaya (E), Western Himalaya (W), Koshi Basin (KB), Langtang Catchment (LC), Garhwal Himalaya (GH), Chenab Basin (CB), Nepal Himalaya (NH), and Indian Himalaya (IH). CI denotes clean-ice glaciers and DC denotes debris-covered glaciers.The dashed line for LC-NH shows area rate change for four different periods during the satellite era for the Langtang catchment.

higher rain-to-snow ratio reduces snow accumulation and enhances melt through latent heat exchange (Immerzeel et al., 2014; Mölg et al., 2014). In addition, autumn and winter temperatures in the catchment are also rising (Supplementary Fig. S12a & Table S9), which likely prolongs the melt season and reinforce melt–albedo feedbacks (Sakai et al., 2009; Pellicciotti et al., 2015). The increase in regional ELA by ~175 from 5360 ± 123 m in the 1960s to 5532 ± 110 m in the 2010s (Fig. 7b & Fig. 10e) could have been driven by such positive feedbacks. This rise in ELA is particularly significant as it now nearly coincides with the median glacier elevation (~5600 m) and increasingly intersects steep and thin icefall areas on the glaciers (Fig. 10e), reducing accumulation area and enhancing melt and thinning. Given that over 70% of the catchment's glacier area lies between 5400 and 6500 m a.s.l. (Fig. 1c), even modest rise in ELA could shift large ice volumes into the ablation zone, reducing the accumulation area ratio (AAR), and thus accelerating mass loss. Thus, rising ELA represents a key driver of glacier recession in the Langtang Catchment.

5.3. Glacier surface elevation change

Glacier area and mass loss in the Langtang Catchment has been accompanied by increased thinning (Fig. 10d). Previous studies which examined the thinning rates of major glaciers in the Langtang Catchment reported a consistent increase in ice loss rates over the last four or five decades, with particularly rapid thinning rates at their low elevations (Pellicciotti et al., 2015; Ragettli et al., 2016; Sugiyama et al., 2013). Our analysis of Hugonnet et al. (2021) datasets confirms this trend, showing an increase in catchment-wide mean thinning rates from -0.41 ± 0.14 m a^{-1} (2000–2004) to -0.77 ± 0.11 m a^{-1} (2015–2019), ~2.5 to 4.5 times higher than the mean thinning rate of -0.16 ± 0.13 m a^{-1} estimated between LIA and 2000 (Fig. 10d).

All glaciers in the catchment thinned between 2000 and 2019. However, debris-covered glaciers showed slightly higher average thinning rates than clean-ice glaciers (Figs. 8a-d & Fig. 10d), despite their thick debris mantle. Earlier studies too showed that debris-covered glaciers in the catchment experience thinning and mass loss rates similar to, or greater than, those of clean-ice glaciers (Pellicciotti et al., 2015; Ragettli et al., 2016). While thick debris mantles are expected to suppress the melt from ice beneath (Østrem, 1959), enhanced thinning on debris-covered tongues is attributed to widespread occurrence of supraglacial ice cliffs and ponds on debris-covered tongues, which locally amplify melt and dominate energy exchanges between debris surface and atmosphere (Buri et al., 2016, 2021, Miles et al., 2016, 2017, 2018, 2022; Pellicciotti et al., 2015; Ragettli et al., 2016; Steiner et al., 2019; Watson et al., 2016). Recent studies further show that increased melt associated with higher ice-cliff abundance leads to similar surface mass balances across debris-covered tongues despite differences in their elevation and air temperatures (Kraaijenbrink and Immerzeel, 2025), highlighting increasing ice-cliff abundance as a key control on mass loss from debris-covered glaciers.

Thinning progressively extending to higher elevations, including icefall and accumulation areas of the glaciers, also indicate a widespread mass loss occurring in the catchment (Figs. 8a–d), consistent with observations across Nepal Himalaya (King et al., 2017; Sunako et al., 2023). Extensive glacier thinning reduces surface slopes (Benn et al., 2012; Quincey et al., 2009), which in turn lowers driving stress, leading to slower ice flow and an expansion of stagnant ice areas (Cuffey and Paterson, 2010; Dehecq et al., 2019). Ultimately, these processes are likely to cause the physical detachment of long debris-covered tongues and a bimodal hypsometry in large valley glaciers.

5.4. Changes in glacier dynamics

Analysis of ITS_LIVE derived glacier surface velocity time series for 1988–2022 shows a clear and sustained slowdown of glaciers in the Langtang catchment, despite notable interannual variability (Figs. 9a-e & Supplementary Fig. S14). Since the early 2000s, flow velocities have declined consistently on both clean-ice and debris-covered glaciers (Supplementary Figs. S14-S15), with tongues of all debris-covered glaciers becoming near-stagnant (flow speed <5 m a^{-1}) in the lower and middle reaches where thinning rates were substantial (Figs. 8a–d & Supplementary Fig. S12). The ITS_LIVE derived flow velocities align with earlier estimates for debris-covered glaciers in the catchment derived using different methods and datasets (e.g. 1.6–7 m a^{-1} for 2008–2009; Ragettli et al., 2016 and 1–3.5 m a^{-1} for 2013–2018; Kraaijenbrink and Immerzeel, 2025). The catchment-wide slowdown in flow velocities is further consistent with the broader regional patterns of glacier slow down observed across Nepalese Himalaya (decrease from -1.8 to -2.2 m a^{-1} dec^{-1}, between 2000 and 2017; Dehecq et al., 2019).

The observed slowdown in glacier surface velocities across the catchment is primarily driven by sustained thinning and the resulting reduction in driving stress (Section 5.3). The pronounced decline in ice flow on debris-covered tongues between 1988 and 2023, leading to stagnation in their middle and lower reaches, can also be attributed to a decreasing mass flux from the accumulation areas due to growing disconnection and fragmentation between active ice and debris-covered tongues (Fig. 5a), together with extensive thinning of up to ~2.5 m a^{-1} (Figs. 8a–d). Slow moving (<10 m a^{-1}), gently sloping (<6–8°) glacier tongues under persistent negative mass-balance regimes favour and promote the growth and expansion of the supraglacial ponds and ice cliffs and redistribution of debris locally (Miles et al., 2016; Sakai et al., 2002; Thompson et al., 2016). Our geomorphological mapping indicates that these features are widespread and have increased across debris-covered tongues throughout the study period (Supplementary Fig. S17 & Table S8), consistent with previous findings. In turn, the expansion of ponds and ice cliffs enhances ablation and thinning (Section 5.3), further suppressing glacier dynamics and reinforcing the observed slowdown (Taylor and Carr, 2019).

5.5. Modulation of glacier response to climatic factors

While climate forcing, particularly warming temperatures at higher elevations has supposedly driven widespread ice mass loss and glacier area change across the Langtang Catchment, individual glacier response could be strongly modulated by their glacier geometry, elevation distribution, and presence or absence of debris cover, resulting in a heterogeneous pattern of glacier change under similar climatic forcing (Thakuri et al., 2014; King et al., 2017; Bhattacharya et al., 2021, 2023). To explore this, we examine relationships between glacier area change, surface mass balance (SMB), and key topographic parameters using correlation matrix (Figs. 12a-c).

The correlation matrix reveals that glacier area change is associated negatively with the elevation range, initial area, debris coverage, and positively with median elevation (Fig. 12b). Weak but significant negative correlation between area change rate and glacier area and elevation range indicates that larger glaciers spanning wider elevation ranges experience slower rates of area loss, likely due to their greater climatic buffering and longer response times (Jóhannesson et al., 1989; Bahr et al., 1998; Paul et al., 2004; Pelto, 2010; Benn and Evans, 2010; Azam et al., 2018). Similarly, significant negative correlation between area change and debris cover percentage suggests that higher debris coverage delayed their geometric response to area loss, consistent with previous observations in the Himalaya (Scherler et al., 2011; Bajracharya et al., 2014). However, some debris-covered valley glaciers with a large elevation range (e.g. Lirung and Langshisha) now exhibit area loss rates comparable to clean-ice glaciers due to increased fragmentation and disconnection. Area loss rates show no significant correlation with slope and aspect; however, we found that glaciers facing southeast-to-southwest with slopes of 20–35° experienced higher loss rates (~1.5–1.8% a^{-1}). This aligns with physical expectations: steeper slopes host thinner ice, where similar thinning rate translates to greater areal reduction (Linsbauer et al., 2012; Anderson et al., 2018).

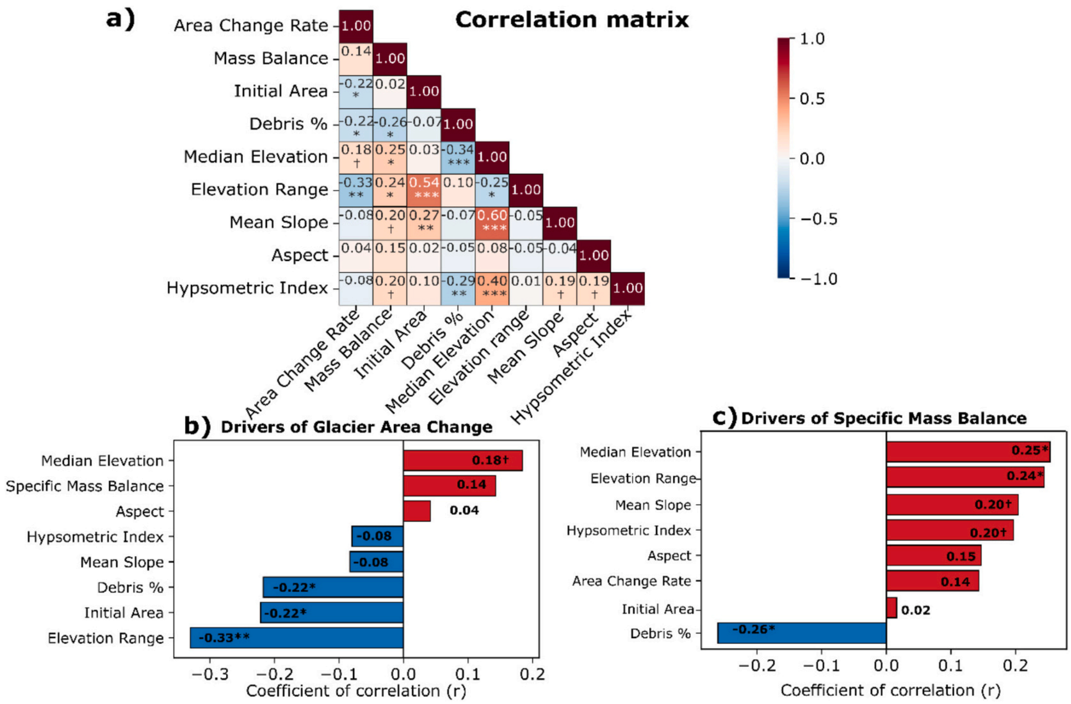

Fig. 12. (a). Correlation matrix for non-climatic (morphology) controls on glacier area change and surface mass balance (SMB). (b). drivers of glacier area change. (c). drivers of SMB. Statistically significant correlations are marked with '***', '**', '*', and '+' for 99.9%, 99%, 95%, and 90%, confidence interval, respectively.

SMB on the other hand, is characterized by more complex and weaker relationships with median elevation, elevation range, slope, and hypsometric index (Fig. 12c). Weak but significant positive correlation between SMB and median elevation indicates that glaciers located at higher elevation are less affected by regional mass loss due to colder temperatures, consistent with regional observations (Bolch et al., 2012; Bhattacharya et al., 2023). In contrast, glaciers with a greater elevation range and a high hypsometric index (BH or VBH glaciers) lost more mass. This is because their larger volume of ice extends down to lower and more warmer elevations where melting is pronounced. Although SMB shows no correlation with glacier area, glaciers with the size (1–2 km^2) and larger glaciers (>5 km^2) exhibited higher mean mass loss (Supplementary Fig. S13b), likely because most of their ice mass is located at the lower elevation and exposed to higher temperatures and thus to more melting and thinning. This is consistent with results from other mountain regions (Brun et al., 2017; Paul and Haeberli, 2008).

Glacier slope also exerts a strong influence on SMB, indicating that steep glaciers are less affected by regional mass loss in the catchment. This is likely because steep slopes enhance ice flow enabling faster dynamic adjustment to climatic forcing (Benn and Evans, 2010; Davaze et al., 2020). However, ongoing glacier thinning (Figs. 8a-d & Fig. 10d) may alter glacier mean slopes, potentially reconfiguring ice flow and modifying future change rates and SMB. Although glacier aspects are known to play crucial role in glacier mass loss in the Himalaya (Racoviteanu et al., 2022; Thakuri et al., 2014), no significant relationship is observed between SMB and glacier aspect here, likely because of the use of mean aspect in our analysis rather than terminal aspect, where most ablation occurs. SMB further shows significant negative correlation with the debris-cover percentage of the glacier, suggesting that glaciers with a larger percentage of debris cover tend to experience less negative SMB. However, this contradicts with the geodetic mass balance obtained from Hugonnet et al. (2021) and regional trends, as debris-covered glaciers in the Langtang Catchment typically display comparable or greater surface lowering and SMB rates (Pellicciotti et al., 2015; Ragettli et al., 2016). This might be due to the limited number of debris-covered glaciers present in the catchment compared to the clean-ice which could potentially reduce the statistical robustness of the relationship because of smaller sample size.

5.6. Glacier fragmentation and disconnection and their impacts on glacier change

Our multitemporal glacier mapping showed increasing glacier fragmentation, disconnection, and tributary separation in the Langtang catchment over the study period (Fig. 5a & Supplementary Table S8). Disconnections and fragmentations are primarily driven by significant thinning in steep ice fall areas on the glacier and the rising ELA increasingly intersecting with these steep, thinned ice and heavily crevassed icefall areas (Fig. 10e & Supplementary Fig. S10). Tributary separation, which also contributes to glacier fragmentation, is largely caused by sustained retreat of tributary glaciers from their main trunks, reducing dynamic coupling between flow units (Rowan et al., 2015; Davies et al., 2022).

Fragmentation and disconnections not only increase numbers of smaller glaciers but also strongly affect glacier dynamics in the catchment. For instance, fragmented and disconnected glaciers such as Lirung, Yala, and Langshisha exhibited higher area and volume loss rates, enhanced surface thinning, and reduced flow velocities compared to the glaciers which have only undergone shrinkage (intact hereafter; Figs. 13c-f). This is expected as disconnection and fragmentation disrupt mass transfer from accumulation to ablation zones, limiting mass replenishment and sustaining negative mass balances in the ablation zones (Anderson et al., 2018; Dehecq et al., 2019).

Fragmentation and disconnection further expose underlying bedrock within key flow units, as observed on Yala and Lirung Glaciers (Figs. 13a-b), enhancing albedo-melt feedback (Jiskoot et al., 2009; Jiskoot and Mueller, 2012). Once completely disconnected from accumulation zones, glacier tongues stagnate and undergo rapid downwasting, as exemplified by the debris-covered tongue of Lirung Glacier (Fig. 13b). As discussed in Section 5.4, stagnation of debris-covered tongue further promotes the formation and growth of supraglacial ponds and ice cliffs, which act as localized melt hotspots (Benn et al., 2012; Ragettli et al., 2016; Buri et al., 2021; Kneib et al., 2023; Nuimura et al., 2017; Steiner et al., 2019). This accelerates more mass loss

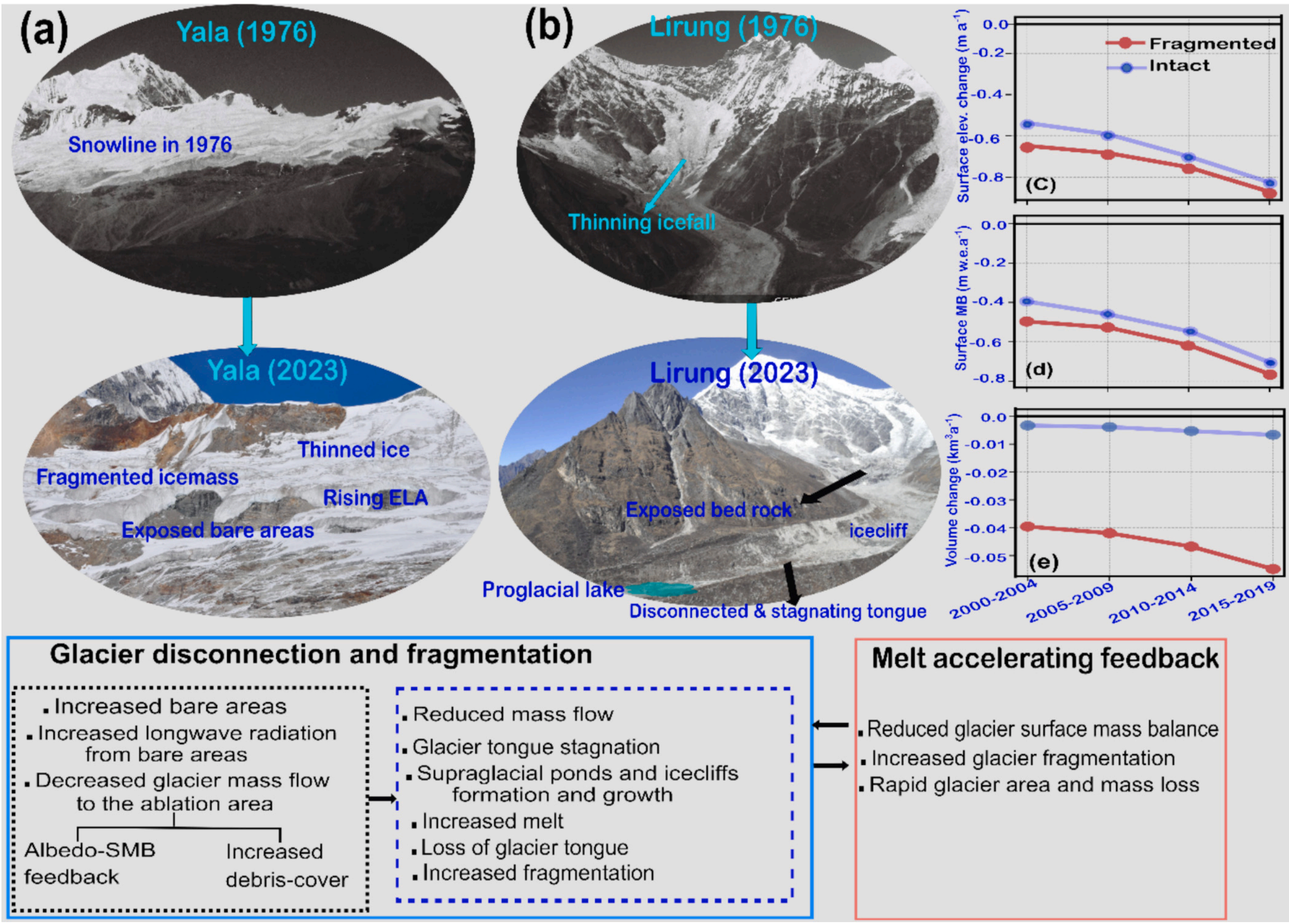

Fig. 13. Some key processes and feedback mechanisms driving long-term glacier evolution and surface changes in the Langtang Catchment. (a-b) Historical and contemporary images of the Yala and Lirung Glaciers illustrate striking glacier retreat, surface lowering, and expansion of debris-cover over the period (1970s –2023). Both glaciers have undergone disconnection and fragmentation and shown upward migration of the snowline, increased bare areas and bed rock exposure. (c-e) Average rates of surface thinning, SMB, and volume change between fragmented and intact glaciers.

and thinning, and on low slope, plateau type glacier like Yala, further thinning can reinforce SMB-elevation feedback.

Tributary separations in large compound valley glaciers such as Langtang and Langshisha have similar effects, reducing the effective accumulation area of the main trunk glacier, thereby accelerating recession and fragmentation and slowing down of ice flow in the ablation zones. Smaller, fragmented glaciers experience disproportionately higher area and mass loss compared to larger compound valley glaciers (Supplementary Figs. S13a-c), consistent with regional and global observations (Bhattacharya et al., 2023; Fischer et al., 2015).

These processes also promote the expansion of the debris-covered area in the ablation zone by exposing previously buried debris through prolonged thinning, downwasting and reduced ice flow (Bhattacharya et al., 2023). Progressive fragmentation and disconnection initiate a positive feedback loop involving reduced ice flux to the ablation zone, debris tongue stagnation, enhanced debris exposure, and intensified melt via albedo-melt feedback, the growth of ice cliffs and supraglacial ponds. Together, these feedbacks accelerate glacier downwasting and eventual glacier disintegration as shown in Figs. 13a-b.

5.7. Implications of this study

Our long-term, multi-temporal assessment of glacier change in the Langtang Catchment (LIA–2023) provides a centennial-scale perspective on glacier change and evolution. The resulting time-specific glacier inventories offer robust constraints for glacier modelling studies of mass balance, landscape evolution, and cryosphere–climate interactions and are directly applicable to other Himalayan regions experiencing similar climatic and glacio-geomorphic changes, supporting assessments of glacier retreat impacts on ecosystems and human societies. For the first time, we systematically mapped and quantified glacier fragmentation, disconnection, and separation, identifying their key drivers and impacts on glacier change, particularly for debris-covered glaciers that are widespread in the Himalaya. Our results underscore the need to explicitly incorporate these processes into regional glacier assessments under warming climate scenarios, as they disproportionately affect long, low-gradient debris-covered glaciers and are likely to become a dominant mode of glacier recession across High Mountain Asia (Rowan et al., 2015, 2021; Shea et al., 2015).

6. Conclusions

This study provides the first comprehensive, long-term assessment of glacier change in the Langtang Catchment using multitemporal, multisource datasets. We reconstructed LIA glacier extents for all glaciers based on moraine ridge crests and trimlines, identifying 58 glaciers covering ~190.21 ± 3.84 km^2 during the LIA. By 2023, 115 glaciers covering 111.43 ± 2.11 km^2 were mapped. This represents a ~ 41.5% reduction in glacier area and a near doubling in glacier number between LIA and 2023. Concurrently, debris-coverage in the catchment increased by 2.11 ± 1.31 km^2 (7.3%) due to rapid mass loss and debris supply from deglaciating glacier surfaces. An inverse relationship was observed between glacier size and area-loss rate, with small clean-ice glaciers shrinking more rapidly than larger debris-covered glaciers. Glacier area loss accelerated more than fourfold, from 0.11% a^{-1} (LIA–1964) to 0.49% a^{-1} (1964–2023), with the highest retreat rates occurring between 2000 and 2016 (0.79% a^{-1}). However, long-term area change rate was sensitive to the chosen LIA maximum age (~1300–1910 CE) and varied substantially (0.025–0.32% a^{-1}) resulting in at 1.5 to 20-fold increase when compared to (1964–2003 CE) area change rates.

Changes in glacier area, SMB, and surface elevation change were congruent with enhanced warming of ~0.3 °C dec^{-1} over the glacierized area > 4000 m a.s.l between 1960 and 2023 and a rising regional equilibrium-line altitude (ELA; from 5360 ± 123 m in the 1960s to 5532 ± 110 m in the 2010s). Glacier size, topographic characteristics, hypsometry, and surface conditions modulated glaciers' response to climate change and produced highly heterogeneous rates of changes across glaciers in the catchment.

The rising ELA increasingly intersecting with the steep, narrow, thin ice, and heavily crevassed icefall areas, is driving glacier fragmentation and disconnections in the catchment. We mapped 26 fragmentations, 13 disconnections, and 14 separations across the glaciers in the catchment in 2023 CE. Fragmentation results in substantial surface area reductions and increased exposure of bedrock and bare areas on the glacier, which enhances melting of the glaciers through albedo-melt feedbacks as well as increases the area loss rates as smaller glaciers recede faster compared to the larger ones. Disconnection in large valley glaciers separate ablation areas (debris-cover tongue) from the active accumulation zones, driving stagnation of the debris tongue. Stagnation of gently sloping debris tongues promotes development of supraglacial ponds and ice cliffs which further enhances down-wasting and thinning, eventually leading to their degradation as evidenced on Lirung Glacier, where progressive degradation is already underway.

Glacier recession through fragmentation and disconnection will become increasingly widespread in the Himalaya under warming climate with critical implications on future glacier evolution and regional hydrology. We emphasize the urgent need for detailed regional assessments of glacier fragmentation and disconnection in the region to better quantify their impacts on meltwater availability and glacier stability. We also emphasize that these processes must be integrated into regional and catchment scale glacier models, as they significantly alter glacier behaviour by changing surface energy balance, albedo, and geometry, factors crucial for accurate future projections.

CRediT authorship contribution statement

Gunjan Silwal: Writing – review & editing, Writing – original draft, Visualization, Methodology, Investigation, Funding acquisition, Formal analysis, Data curation, Conceptualization. **Bethan Davies:** Writing – review & editing, Supervision, Conceptualization. **J. Rachel Carr:** Writing – review & editing, Supervision, Conceptualization. **Owen King:** Writing – review & editing, Supervision, Data curation, Conceptualization. **Sammie Buzzard:** Writing – review & editing, Supervision. **Jonathan L. Carrivick:** Writing – review & editing, Supervision, Methodology. **Prashant Baral:** Writing – review & editing.

Declaration of competing interest

The authors declare the following financial interests/personal relationships which may be considered as potential competing interests:

One of the (co-) authors is a member of the editorial board. If there are other authors, they declare that they have no known competing financial interests or personal relationships that could have appeared to influence the work reported in this paper.

Acknowledgements

This study has been supported by the Natural Environmental Research Council (NERC)-funded ONE Planet Doctoral Training Partnership (NE/S007512/1). The authors also thank Dr. Atanu Bhattacharya for access to the Corona KH4 and Hexagon KH9 orthoimages. GS acknowledges fieldwork grant received from the Quaternary Research Association (QRA). We also thank Dawa Sherpa from Kathmandu University and Himalayan Research Expedition (HRE) for their excellent fieldwork support.

Appendix A. Supplementary data

Supplementary data to this article can be found online at https://doi.org/10.1016/j.gloplacha.2026.105555.

Data availability

All data used in the study were sourced from publicly available data repositories (see Methods for further details). The glacier outlines from different periods and any additional data related to the analysis may be obtained through the direct contact with the corresponding author.

References

Ageta, Y., Higuchi, K., 1984. Estimation of mass balance components of a summer-accumulation type glacier in the Nepal Himalaya. Geogr. Ann. Ser. B 66 (3), 249–255.

Allen, S., Frey, H., Haeberli, W., Huggel, C., Chiarle, M., Geertsema, M., 2022. Assessment principles for glacier and permafrost hazards in mountain regions. In: Oxford Research Encyclopedia of Natural Hazard Science.

Allison, E.A., 2015. The spiritual significance of glaciers in an age of climate change. Wiley Interdiscip. Rev. Clim. Chang. 6 (5), 493–508.

Anderson, R.S., Anderson, L.S., Armstrong, W.H., Rossi, M.W., Crump, S.E., 2018. Glaciation of alpine valleys: the glacier–debris-covered glacier–rock glacier continuum. Geomorphology 311, 127–142.

Azam, M.F., Wagnon, P., Berthier, E., Vincent, C., Fujita, K., Kargel, J.S., 2018. Review of the status and mass changes of Himalayan-Karakoram glaciers. J. Glaciol. 64 (243), 61–74.

Bahr, D.B., Pfeffer, W.T., Sassolas, C., Meier, M.F., 1998. Response time of glaciers as a function of size and mass balance: 1. Theory. J. Geophys. Res. Solid Earth 103 (B5), 9777–9782.

Bajracharya, S.R., Shrestha, B.R., 2011. The status of glaciers in the Hindu Kush-Himalayan region. International Centre for Integrated Mountain Development (ICIMOD).

Bajracharya, S.R., Maharjan, S.B., Shrestha, F., 2014. Understanding dynamics of Himalayan glaciers: scope and challenges of remote sensing. In: Dadhwal, V.K., Diwakar, P.G., Seshasai, M.V.R., Raju, P.L.N., Hakeem, A. (Eds.), *ISPRS Technical Commission VIII Symposium* (Vols 40–8, pp. 1283–1289). https://doi.org/10.5194/isprsarchives-XL-8-1283-2014.

Bajracharya, S.R., Maharjan, S.B., Shrestha, F., Guo, W., Liu, S., Immerzeel, W., Shrestha, B., 2015. The glaciers of the Hindu Kush Himalayas: current status and observed changes from the 1980s to 2010. Int. J. Water Resour. Develop. 31 (2), 161–173. https://doi.org/10.1080/07900627.2015.1005731.

Barnard, P.L., Owen, L.A., Finkel, R.C., Asahi, K., 2006. Landscape response to deglaciation in a high relief, monsoon-influenced alpine environment, Langtang Himal, Nepal. Quat. Sci. Rev. 25 (17), 2162–2176. https://doi.org/10.1016/j.quascirev.2006.02.002.

Benn, D., Evans, D.J., 2010. Glaciers and Glaciation, 2nd ed. Routledge. https://doi.org/10.4324/9780203785010.

Benn, D.I., Bolch, T., Hands, K., Gulley, J., Luckman, A., Nicholson, L.I., Quincey, D., Thompson, S., Toumi, R., Wiseman, 2012. Response of debris-covered glaciers in the Mount Everest region to recent warming, and implications for outburst flood hazards. Earth Sci. Rev. 114 (1–2), 156–174. https://doi.org/10.1016/j.earscirev.2012.03.008.

Bhambri, R., Bolch, T., Chaujar, R.K., Kulshreshtha, S.C., 2011. Glacier changes in the Garhwal Himalaya, India, from 1968 to 2006 based on remote sensing. J. Glaciol. 57 (203), 543–556.

Bhattacharya, A., Bolch, T., Mukherjee, K., King, O., Menounos, B., Kapitsa, V., Neckel, N., Yang, W., Yao, T., 2021. High Mountain Asian glacier response to climate revealed by multi-temporal satellite observations since the 1960s. Nat. Commun. 12 (1), 1–13. https://doi.org/10.1038/s41467-021-24180-y.

Bhattacharya, A., Mukherjee, K., King, O., Karmakar, S., Remya, S.N., Kulkarni, A.V., Bolch, T., 2023. Influence of climate and non-climatic attributes on declining glacier mass budget and surging in Alaknanda Basin and its surroundings. Glob. Planet. Chang. 230, 104260.

Bolch, T., Buchroithner, M., Pieczonka, T., Kunert, A., 2008. Planimetric and volumetric glacier changes in the Khumbu Himal, Nepal, since 1962 using Corona, Landsat TM and ASTER data. J. Glaciol. 54 (187), 592–600.
Bolch, T., Yao, T., Kang, S., Buchroithner, M.F., Scherer, D., Maussion, F., Schneider, C., 2010. A glacier inventory for the western Nyainqentanglha Range and the Nam Co Basin, Tibet, and glacier changes 1976–2009. Cryosphere 4 (3), 419–433.
Bolch, T., Pieczonka, T., Benn, D.I., 2011. Multi-decadal mass loss of glaciers in the Everest area (Nepal Himalaya) derived from stereo imagery. Cryosphere 5 (2), 349–358.
Bolch, T., Kulkarni, A., Kääb, A., Huggel, C., Paul, F., Cogley, J.G., Frey, H., Kargel, J.S., Fujita, K., Scheel, M., Bajracharya, S., Stoffel, M., Kaab, A., Huggel, C., Paul, F., Cogley, J.G., Frey, H., Kargel, J.S., Fujita, K., Stoffel, M., 2012. The state and fate of himalayan glaciers. Science 336 (6079), 310–314. https://doi.org/10.1126/science.1215828.
Bosson, J.B., Huss, M., Cauvy-Fraunié, S., Clément, J.C., Costes, G., Fischer, M., Arthaud, F., 2023. Future emergence of new ecosystems caused by glacial retreat. Nature 620 (7974), 562–569.
Brun, F., Berthier, E., Wagnon, P., Kääb, A., Treichler, D., 2017. A spatially resolved estimate of High Mountain Asia glacier mass balances from 2000 to 2016. Nat. Geosci. 10 (9), 668–673.
Brun, F., Wagnon, P., Berthier, E., Jomelli, V., Maharjan, S.B., Shrestha, F., Kraaijenbrink, P.D.A.A., 2019. Heterogeneous influence of glacier morphology on the mass balance variability in High Mountain Asia. J. Geophys. Res.: Earth Surf. 124 (6), 1331–1345. https://doi.org/10.1029/2018JF004838.
Buri, P., Miles, E.S., Steiner, J.F., Immerzeel, W.W., Wagnon, P., Pellicciotti, F., 2016. A physically based 3-D model of ice cliff evolution over debris-covered glaciers. J. Geophys. Res. Earth Surf. 121 (12), 2471–2493.
Buri, P., Miles, E.S., Steiner, J.F., Ragettli, S., Pellicciotti, F., 2021. Supraglacial ice cliffs can substantially increase the mass loss of debris-covered glaciers. Geophys. Res. Lett. 48 (6), e2020GL092150.
Bussard, J., Reynard, E., 2023. Conservation of World Heritage glacial landscapes in a changing climate: the Swiss Alps Jungfrau-Aletsch case. Int. J. Geoheritage Parks 11 (4), 535–552.
Carrivick, J.L., Tweed, F.S., 2016. A global assessment of the societal impacts of glacier outburst floods. Glob. Planet. Chang. 144, 1–16.
Carrivick, J.L., Boston, C.M., King, O., James, W.H.M., Quincey, D.J., Smith, M.W., Grimes, M., Evans, J., 2019. Accelerated volume loss in glacier ablation zones of NE Greenland, Little Ice Age to present. Geophys. Res. Lett. 46 (3), 1476–1484.
Carrivick, J.L., James, W.H.M., Grimes, M., Sutherland, J.L., Lorrey, A.M., 2020. Ice thickness and volume changes across the Southern Alps, New Zealand, from the little ice age to present. Sci. Rep. 10 (1), 13392.
Carrivick, J.L., Andreassen, L.M., Nesje, A., Yde, J.C., 2022. A reconstruction of Jostedalsbreen during the Little Ice Age and geometric changes to outlet glaciers since then. Quat. Sci. Rev. 284, 107501. https://doi.org/10.1016/j.quascirev.2022.107501.
Carrivick, J.L., Davies, M., Wilson, R., Davies, B.J., Gribbin, T., King, O., Rabatel, A., García, J.L., Ely, J.C., 2024. Accelerating Glacier Area loss across the Andes since the Little Ice Age. Geophys. Res. Lett. 51 (13), 1–12. https://doi.org/10.1029/2024GL109154.
Chinn, T.J., Heydenrych, C., Salinger, M.J., 2005. Use of the ELA as a practical method of monitoring glacier response to climate in New Zealand's Southern Alps. J. Glaciol. 51, 85–95.
Cook, E.R., Krusic, P.J., Jones, P.D., 2003. Dendroclimatic signals in long tree-ring chronologies from the Himalayas of Nepal. Int. J. Climatol. 23 (7), 707–732.
Cuffey, K.M., Paterson, W.S.B., 2010. The Physics of Glaciers. Academic Press.
Davaze, L., Rabatel, A., Dufour, A., Hugonnet, R., Arnaud, Y., 2020. Region-wide annual glacier surface mass balance for the European Alps from 2000 to 2016. Front. Earth Sci. 8, 149.
Davies, B., Bendle, J., Carrivick, J., McNabb, R., McNeil, C., Pelto, M., Campbell, S., Holt, T., Ely, J., Markle, B., 2022. Topographic controls on ice flow and recession for Juneau Icefield (Alaska/British Columbia). Earth Surf. Process. Landf. 47 (9), 2357–2390.
Davies, B., McNabb, R., Bendle, J., Carrivick, J., Ely, J., Holt, T., Markle, B., McNeil, C., Nicholson, L., Pelto, M., 2024. Accelerating glacier volume loss on Juneau Icefield driven by hypsometry and melt-accelerating feedbacks. Nat. Commun. 15 (1), 5099. https://doi.org/10.1038/s41467-024-49269-y.
Dehecq, A., Gourmelen, N., Gardner, A.S., Brun, F., Goldberg, D., Nienow, P.W., Berthier, E., Vincent, C., Wagnon, P., Trouvé, E., 2019. Twenty-first century glacier slowdown driven by mass loss in High Mountain Asia. Nat. Geosci. 12 (1), 22–27. https://doi.org/10.1038/s41561-018-0271-9.
Farinotti, D., Huss, M., Fürst, J.J., Landmann, J., Machguth, H., Maussion, F., Pandit, A., 2019. A consensus estimate for the ice thickness distribution of all glaciers on Earth. Nat. Geosci. 12 (3), 168–173. https://doi.org/10.1038/s41561-019-0300-3.
Farr, T.G., Rosen, P.A., Caro, E., Crippen, R., Duren, R., Hensley, S., Kobrick, M., Paller, M., Rodriguez, E., Roth, L., 2007. The shuttle radar topography mission. Rev. Geophys. 45 (2).
Fischer, M., Huss, M., Hoelzle, M., 2015. Surface elevation and mass changes of all Swiss glaciers 1980–2010. Cryosphere 9 (2), 525–540.
Forster, P.M., Smith, C., Walsh, T., Lamb, W.F., Lamboll, R., Hall, B., Zhai, P., 2024. Indicators of Global climate Change 2023: annual update of key indicators of the state of the climate system and human influence. Earth Syst. Sci. Data 16 (6), 2625–2658.
Fox-Kemper, B., Aðalgeirsdóttir, G., 2023. IPCC 6 Chapter 9 SM Ocean, Cryosphere, and Sea Level Change Supplementary Material Coordinating Lead Authors: Lead Authors.
Fujita, K., Nuimura, T., 2011. Spatially heterogeneous wastage of Himalayan glaciers. Proc. Natl. Acad. Sci. USA 108 (34), 14011–14014. https://doi.org/10.1073/pnas.1106242108.
Fujita, K., Thompson, L.G., Ageta, Y., Yasunari, T., Kajikawa, Y., Sakai, A., Takeuchi, N., 2006. Thirty-year history of glacier melting in the Nepal Himalayas. J. Geophys. Res. Atmos. 111 (D3).
Gardelle, J., Berthier, E., Arnaud, Y., Kääb, A., 2013. Region-wide glacier mass balances over the Pamir-Karakoram-Himalaya during 1999–2011. Cryosphere 7 (4), 1263–1286.
Gardner, A., Fahnestock, M., Scambos, T., 2022. MEaSUREs ITS_LIVE Regional Glacier and Ice Sheet Surface Velocities, Version 1. NASA National Snow and Ice Data Center Distributed Active Archive Center. https://doi.org/10.5067/6II6VW8LLWJ7.
Gardner, A.S., Moholdt, G., Scambos, T., Fahnstock, M., Ligtenberg, S., van den Broeke, M., Nilsson, J., 2018. Increased West Antarctic and unchanged East Antarctic ice discharge over the last 7 years. Cryosphere 12 (2), 521–547. https://doi.org/10.5194/tc-12-521-2018.
Glasser, N.F., Jansson, K.N., Harrison, S., Rivera, A., 2005. Geomorphological evidence for variations of the North Patagonian Icefield during the Holocene. Geomorphology 71 (3–4), 263–277.
Grove, J.M., 2019. The Little Ice Age. Routledge.
Harrison, S., Kargel, J.S., Huggel, C., Reynolds, J., Shugar, D.H., Betts, R.A., Emmer, A., Glasser, N., Haritashya, U.K., Klimeš, J., 2018. Climate change and the global pattern of moraine-dammed glacial lake outburst floods. Cryosphere 12 (4), 1195–1209.
Hugonnet, R., Mcnabb, R., Berthier, E., Menounos, B., Nuth, C., Girod, L., Farinotti, D., Huss, M., Dussaillant, I., Brun, F., Kääb, A., 2021. Accelerated global glacier mass loss in the early twenty-first century. Nature 592 (7856), 726–731. https://doi.org/10.1038/s41586-021-03436-z.
Immerzeel, W.W., Petersen, L., Ragettli, S., Pellicciotti, F., 2014. The importance of observed gradients of air temperature and precipitation for modeling runoff from a glacierized watershed in the Nepalese Himalayas. Water Resour. Res. 50 (3), 2212–2226.
Immerzeel, W.W., Lutz, A.F., Andrade, M., Bahl, A., Biemans, H., Bolch, T., Hyde, S., Brumby, S., Davies, B.J., Elmore, A.C., Emmer, A., Feng, M., Fernández, A., Haritashya, U., Kargel, J.S., Koppes, M., Kraaijenbrink, P.D.A., Kulkarni, A.V., Mayewski, P.A., Baillie, J.E.M., 2020. Importance and vulnerability of the world's water towers. Nature 577 (7790), 364–369. https://doi.org/10.1038/s41586-019-1822-y.
Jackson, M., Azam, M.F., Baral, P., Benestad, R., Brun, F., Muhammad, S., Pradhananga, S., Shrestha, F., Steiner, J.F., Thapa, A., 2023. Consequences of climate change for the cryosphere in the Hindu Kush Himalaya. In: Wester, P., Chaudhary, S., Chettri, N., Jackson, M., Maharjan, A., Nepal, S., Steiner, J.F. (Eds.), Water, Ice, Society, and Ecosystems in the Hindu Kush Himalaya: An Outlook. ICIMOD, pp. 17–71. https://doi.org/10.53055/ICIMOD.1030.
Jiskoot, H., Mueller, M.S., 2012. Glacier fragmentation effects on surface energy balance and runoff: field measurements and distributed modelling. Hydrol. Process. 26 (12), 1861–1875.
Jiskoot, H., Curran, C.J., Tessler, D.L., Shenton, L.R., 2009. Changes in Clemenceau Icefield and Chaba Group glaciers, Canada, related to hypsometry, tributary detachment, length-slope and area-aspect relations. Ann. Glaciol. 50 (53), 133–143. https://doi.org/10.3189/172756410790595796.
Jóhannesson, T., Raymond, C., Waddington, E.D., 1989. Time–scale for adjustment of glaciers to changes in mass balance. J. Glaciol. 35 (121), 355–369.
Kayastha, R.B., Harrison, P., 2008. Changes of the equilibrium-line altitude since the Little Ice Age in the Nepalese Himalaya. Ann. Glaciol. 48, 93–99. https://doi.org/10.3189/172756408784700581.
King, O., Quincey, D.J., Carrivick, J.L., Rowan, A.V., 2017. Spatial variability in mass loss of glaciers in the Everest region, Central Himalayas, between 2000 and 2015. Cryosphere 11 (1), 407–426.
King, O., Dehecq, A., Quincey, D., Carrivick, J., 2018. Contrasting geometric and dynamic evolution of lake and land-terminating glaciers in the central Himalaya. Glob. Planet. Chang. 167 (November 2017), 46–60. https://doi.org/10.1016/j.gloplacha.2018.05.006.
King, O., Turner, A.G.D., Quincey, D.J., Carrivick, J.L., 2020. Morphometric evolution of Everest region debris-covered glaciers. Geomorphology 371 (November 2015), 107422. https://doi.org/10.1016/j.geomorph.2020.107422.
Kneib, M., Fyffe, C.L., Miles, E.S., Lindemann, S., Shaw, T.E., Buri, P., Pellicciotti, F., 2023. Controls on ice cliff distribution and characteristics on debris-covered glaciers. Geophys. Res. Lett. 50 (6), e2022GL102444.
Kraaijenbrink, P.D., Bierkens, M.F., Lutz, A.F., Immerzeel, W.W., 2017. Impact of a global temperature rise of 1.5 degrees Celsius on Asia's glaciers. Nature 549 (7671), 257–260.
Kraaijenbrink, P.D.A., Immerzeel, W.W., 2025. Spatial and temporal variability of the surface mass balance of debris-covered glacier tongues. J. Geophys. Res.: Earth Surf. 130 (3), e2024JF007935.
Lange, S., Menz, C., Gleixner, S., Cucchi, M., Weedon, G.P., Amici, A., Bellouin, N., Schmied, H.M., Hersbach, H., Buontempo, C., 2021. WFDE5 over land merged with ERA5 over the ocean (W5E5 v2. 0).
Lee, E., Carrivick, J.L., Quincey, D.J., Cook, S.J., James, W.H.M., Brown, L.E., 2021. Accelerated mass loss of Himalayan glaciers since the Little Ice Age. Sci. Rep. 11 (1), 1–8.
Linsbauer, A., Paul, F., Haeberli, W., 2012. Modeling glacier thickness distribution and bed topography over entire mountain ranges with GlabTop: Application of a fast and robust approach. J. Geophys. Res.: Earth Surf. 117 (F3).
Losapio, G., Lee, J.R., Fraser, C.I., Gillespie, M.A., Kerr, N.R., Zawierucha, K., Brown, L. E., 2025. Impacts of deglaciation on biodiversity and ecosystem function. Nat. Rev. Biodivers. 1–15.

Lutz, A.F., 2016. Impact of Climate Change on the Hydrology of High Mountain Asia.
Lutz, A.F., Immerzeel, W.W., Siderius, C., Wijngaard, R.R., Nepal, S., Shrestha, A.B., Wester, P., Biemans, H., 2022. South Asian agriculture increasingly dependent on meltwater and groundwater. Nat. Clim. Chang. https://doi.org/10.1038/S41558-022-01355-Z.
Marzeion, B., Jarosch, A.H., Hofer, M., 2012. Past and future sea-level change from the surface mass balance of glaciers. Cryosphere 6 (6), 1295–1322. https://doi.org/10.5194/tc-6-1295-2012.
Marzeion, B., Hock, R., Anderson, B., Bliss, A., Champollion, N., Fujita, K., Huss, M., Immerzeel, W.W., Kraaijenbrink, P., Malles, J., Maussion, F., Radić, V., Rounce, D.R., Sakai, A., Shannon, S., Wal, R., Zekollari, H., 2020. Partitioning the uncertainty of ensemble projections of global glacier mass change. Earth's Future 8 (7). https://doi.org/10.1029/2019EF001470.
Maurer, J.M., Schaefer, J.M., Rupper, S., Corley, A., 2019. Acceleration of ice loss across the Himalayas over the past 40 years. Sci. Adv. 5 (6), eaav7266. https://doi.org/10.1126/sciadv.aav7266.
Maussion, F., Butenko, A., Champollion, N., Dusch, M., Eis, J., Fourteau, K., Gregor, P., Jarosch, A.H., Landmann, J., Oesterle, F., 2019. The open global glacier model (OGGM) v1. 1. Geosci. Model Dev. 12 (3), 909–931.
Mcgrath, D., Sass, L., O'Neel, S., Arendt, A., Kienholz, C., 2017. Hypsometric control on glacier mass balance sensitivity in Alaska and Northwest Canada. Earth's Future 5 (3), 324–336.
Miles, E.S., Willis, I.C., Arnold, N.S., Steiner, J., Pellicciotti, F., 2017. Spatial, seasonal and interannual variability of supraglacial ponds in the Langtang Valley of Nepal, 1999–2013. J. Glaciol. 63 (237), 88–105.
Miles, E.S., Willis, I., Buri, P., Steiner, J.F., Arnold, N.S., Pellicciotti, F., 2018. Surface Pond Energy Absorption across four Himalayan Glaciers Accounts for 1/8 of Total Catchment Ice loss. Geophys. Res. Lett. 45 (19), 10464–10473. https://doi.org/10.1029/2018GL079678.
Miles, E.S., Pellicciotti, F., Willis, I.C., Steiner, J.F., Buri, P., Arnold, N.S., 2016. Refined energy-balance modelling of a supraglacial pond, Langtang Khola, Nepal. Ann. Glaciol. 57 (71), 29–40.
Miles, E.S., Steiner, J.F., Buri, P., Immerzeel, W.W., Pellicciotti, F., 2022. Controls on the relative melt rates of debris-covered glacier surfaces. Environ. Res. Lett. 17 (6), 064004.
Mir, R.A., Jain, S.K., Ahmed, R., Rather, A.F., 2025. A strategic framework for Glacial Lake Outburst Flood (GLOF) risk reduction in the Himalayas under climate change. Discov. Geosci. 3 (1), 143.
Molden, D.J., Shrestha, A.B., Immerzeel, W.W., Maharjan, A., Rasul, G., Wester, P., Wagle, N., Pradhananga, S., Nepal, S., 2022. The Great Glacier and Snow-Dependent Rivers of Asia and Climate Change: Heading for Troubled Waters. In: Water Resources Development and Management. Springer Singapore. https://doi.org/10.1007/978-981-16-5493-0_12.
Mölg, T., Maussion, F., Scherer, D., 2014. Mid-latitude westerlies as a driver of glacier variability in monsoonal High Asia. Nat. Clim. Chang. 4 (1), 68–73.
Mountain Research Initiative EDW Working Group, 2015. Elevation-dependent warming in mountain regions of the world. Nat. Clim. Chang. 5, 424–430. https://doi.org/10.1038/nclimate2563.
Muhammad, S., Thapa, A., 2021. Daily Terra–Aqua MODIS cloud-free snow and Randolph Glacier Inventory 6.0 combined product (M* D10A1GL06) for high-mountain Asia between 2002 and 2019. Earth Syst. Sci. Data 13 (2), 767–776.
Muñoz-Sabater, J., Dutra, E., Agustí-Panareda, A., Albergel, C., Arduini, G., Balsamo, G., Thépaut, J.N., 2021. ERA5-Land: a state-of-the-art global reanalysis dataset for land applications. Earth Syst. Sci. Data 13 (9), 4349–4383.
Nuimura, T., Fujita, K., Sakai, A., 2017. Downwasting of the debris-covered area of Lirung Glacier in Langtang Valley, Nepal Himalaya, from 1974 to 2010. Quat. Int. 455, 93–101. https://doi.org/10.1016/j.quaint.2017.06.066.
Oerlemans, J., 2001. Glaciers and Climate Change. CRC Press.
Oien, R.P., Rea, B.R., Spagnolo, M., Barr, I.D., Bingham, R.G., 2022. Testing the area–altitude balance ratio (AABR) and accumulation–area ratio (AAR) methods of calculating glacier equilibrium-line altitudes. J. Glaciol. 68 (268), 357–368.
Ono, Y., 1985. Recent fluctuations of the Yala (Dakpatsen) Glacier, Langtang Himal, reconstructed from annual moraine ridges. Zeitschrift Fur Gletscherkunde Und Glazialgeologie 21, 251–258.
Østrem, G., 1959. Ice melting under a thin layer of moraine, and the existence of ice cores in moraine ridges. Geogr. Ann. 41 (4), 228–230.
Owen, L.A., Derbyshire, E., Fort, M., 1998. The quaternary glacial history of the himalaya. J. Quat. Sci. 13 (Suppl. 1).
Paul, F., Haeberli, W., 2008. Spatial variability of glacier elevation changes in the Swiss Alps obtained from two digital elevation models. Geophys. Res. Lett. 35 (21).
Paul, F., Kääb, A., Maisch, M., Kellenberger, T., Haeberli, W., 2004. Rapid disintegration of Alpine glaciers observed with satellite data. Geophys. Res. Lett. 31 (21).
Paul, F., Barrand, N.E., Baumann, S., Berthier, E., Bolch, T., Casey, K., Frey, H., Joshi, S. P., Konovalov, V., Le Bris, R., Mölg, N., Nosenko, G., Nuth, C., Pope, A., Racoviteanu, A., Rastner, P., Raup, B., Scharrer, K., Steffen, S., Winsvold, S., 2013. On the accuracy of glacier outlines derived from remote-sensing data. Ann. Glaciol. 54 (63), 171–182. https://doi.org/10.3189/2013AoG63A296.
Pellicciotti, F., Stephan, C., Miles, E., Herreid, S., Immerzeel, W.W., Bolch, T., 2015. Mass-balance changes of the debris-covered glaciers in the Langtang Himal, Nepal, from 1974 to 1999. J. Glaciol. 61 (226), 373–386. https://doi.org/10.3189/2015JoG13J237.
Pellitero, R., Rea, B.R., Spagnolo, M., Bakke, J., Hughes, P., Ivy-Ochs, S., Lukas, S., Ribolini, A., 2015. A GIS tool for automatic calculation of glacier equilibrium-line altitudes. Comput. Geosci. 82, 55–62.
Pelto, M.S., 2010. Forecasting temperate alpine glacier survival from accumulation zone observations. Cryosphere 4 (1), 67–75.
Pradhananga, D., Adhikary, S., Dhakal, B.N., Dhakal, A., Ghimire, A., Dhital, S., Manandhar, S., 2025. Cryosphere change in the warming Himalaya: Snow cover and snowline trends in Nepal's Langtang Basin (1988-2024). J. Tourism Himalayan Adventures 7 (1), 14–26.
Pronk, Jan Bouke, Tobias, Bolch, Owen, King, Bert, Wouters, Douglas, I. Benn, 2021. Contrasting surface velocities between lake-and land-terminating glaciers in the Himalayan region. Cryosphere 15 (12), 5577–5599.
Quincey, D.J., Luckman, A., Benn, D., 2009. Quantification of Everest region glacier velocities between 1992 and 2002, using satellite radar interferometry and feature tracking. J. Glaciol. 55 (192), 596–606.
Qureshi, M.A., Li, Y., Yi, C., Xu, X., 2021. Glacial changes in the Hunza Basin, western Karakoram, since the Little Ice Age. Palaeogeogr. Palaeoclimatol. Palaeoecol. 562, 110086.
Racoviteanu, A.E., Arnaud, Y., Williams, M.W., Manley, W.F., 2015. Spatial patterns in glacier characteristics and area changes from 1962 to 2006 in the Kanchenjunga-Sikkim area, eastern Himalaya. Cryosphere 9 (2), 505–523. https://doi.org/10.5194/tc-9-505-2015.
Racoviteanu, A.E., Glasser, N.F., Robson, B.A., Harrison, S., Millan, R., Kayastha, R.B., Kayastha, R., 2022. Recent evolution of glaciers in the Manaslu region of Nepal from satellite imagery and UAV data (1970–2019). Front. Earth Sci. 9, 767317.
Ragettli, S., Bolch, T., Pellicciotti, F., 2016. Heterogeneous glacier thinning patterns over the last 40 years in Langtang Himal, Nepal. Cryosphere 10 (5), 2075–2097.
Rasul, G., Molden, D., 2019. The global social and economic consequences of mountain cryospheric change. Front. Environ. Sci. 7, 91.
Reinthaler, J., Paul, F., 2023. Using a Web Map Service to map Little Ice Age glacier extents at regional scales. Ann. Glaciol. 64 (92), 206–224.
Reinthaler, J., Paul, F., 2025. Reconstructed glacier area and volume changes in the European Alps since the Little Ice Age. Cryosphere 19 (2), 753–767.
Remya, S.N., Kulkarni, A.V., Pradeep, S., Shrestha, D.G., 2019. Volume estimation of existing and potential glacier lakes, Sikkim Himalaya. India Curr. Sci. 116, 620–627. https://jstor.org/stable/27137905.
Remya, S.N., Nandan, V., Bhattacharya, A., Srinivasalu, P., Mukherjee, K., Raj, B.G., Bolch, T., 2025. Glacier calving and moraine collapse triggered the glacial Lake outburst flood in South Lhonak Lake, Indian Himalaya. Environ. Res. Commun. 7 (11), 115026.
RGI Consortium, 2023. Randolph Glacier Inventory - A Dataset of Global Glacier Outlines, Version 7. NASA National Snow and Ice Data Center Distributed Active Archive Center. https://doi.org/10.5067/F6JMOVY5NAVZ.
Rippin, D.M., Sharp, M., Van Wychen, W., Zubot, D., 2020. Detachment'of icefield outlet glaciers: catastrophic thinning and retreat of the Columbia Glacier (Canada). Earth Surf. Process. Landf. 45 (2), 459–472.
Rowan, A.V., 2017. The 'Little Ice Age' in the Himalaya: a review of glacier advance driven by Northern Hemisphere temperature change. Holocene 27 (2), 292–308. https://doi.org/10.1177/0959683616658530.
Rowan, A.V., Egholm, D.L., Quincey, D.J., Glasser, N.F., 2015. Modelling the feedbacks between mass balance, ice flow and debris transport to predict the response to climate change of debris-covered glaciers in the Himalaya. Earth Planet. Sci. Lett. 430, 427–438.
Rowan, A.V., Egholm, D.L., Quincey, D.J., Hubbard, B., King, O., Miles, E.S., Hornsey, J., 2021. The role of differential ablation and dynamic detachment in driving accelerating mass loss from a debris-covered Himalayan glacier. J. Geophys. Res.: Earth Surf. 126 (9), e2020JF005761.
Sakai, A., Nakawo, M., Fujita, K., 2002. Distribution characteristics and energy balance of ice cliffs on debris-covered glaciers, Nepal Himalaya. Arct. Antarct. Alp. Res. 34 (1), 12–19.
Sakai, A., Nishimura, K., Kadota, T., Takeuchi, N., 2009. Onset of calving at supraglacial lakes on debris-covered glaciers of the Nepal Himalaya. J. Glaciol. 55 (193), 909–917.
Sattar, A., Cook, K.L., Rai, S.K., Berthier, E., Allen, S., Rinzin, S., Bhat, S.Y., 2025. The Sikkim flood of October 2023: drivers, causes, and impacts of a multihazard cascade. Science 387 (6740), eads2659.
Scherler, D., Bookhagen, B., Strecker, M.R., 2011. Spatially variable response of Himalayan glaciers to climate change affected by debris cover. Nat. Geosci. 4 (3), 156–159.
Shea, J.M., Immerzeel, W.W., Wagnon, P., Vincent, C., Bajracharya, S., 2015. Modelling glacier change in the Everest region, Nepal Himalaya. Cryosphere 9 (3), 1105–1128.
Shekhar, M., Bhardwaj, A., Singh, S., Ranhotra, P.S., Bhattacharyya, A., Pal, A.K., Zorzano, M.P., 2017. Himalayan glaciers experienced significant mass loss during later phases of little ice age. Sci. Rep. 7 (1), 10305.
Shiraiwa, T., Watanabe, T., 1991. Late Quaternary glacial fluctuations in the Langtang Valley, Nepal Himalaya, reconstructed by relative dating methods. Arct. Alp. Res. 23 (4), 404–416. https://doi.org/10.2307/1551682.
Shrestha, F., Steiner, J.F., Shrestha, R., Dhungel, Y., Joshi, S.P., Inglis, S., Ashraf, A., Wali, S., Walizada, K.M., Zhang, T., 2023. A comprehensive and version-controlled database of glacial lake outburst floods in High Mountain Asia. Earth Syst. Sci. Data 15, 3941–3961. https://doi.org/10.5194/essd-15-3941-2023.
Steiner, J.F., Buri, P., Miles, E.S., Ragettli, S., Pellicciotti, F., 2019. Supraglacial ice cliffs and ponds on debris-covered glaciers: spatio-temporal distribution and characteristics. J. Glaciol. 65 (252), 617–632. https://doi.org/10.1017/jog.2019.40.
Steiner, J.F., Gurung, T.R., Joshi, S.P., Koch, I., Saloranta, T., Shea, J., Shrestha, A.B., Stigter, E., Immerzeel, W.W., 2021. Multi-year observations of the high mountain water cycle in the Langtang catchment, Central Himalaya. Hydrol. Process. 35 (5), e14189.
Stumm, D., Joshi, S.P., Gurung, T.R., Silwal, G., 2021. Mass balances of Yala and Rikha Samba glaciers, Nepal, from 2000 to 2017. Earth Syst. Sci. Data 13 (8), 3791–3818. https://doi.org/10.5194/essd-13-3791-2021.

Sugiyama, S., Kukui, K., Fujita, K., Tone, K., Yamaguchi, S., 2013. Changes in ice thickness and flow velocity ofYala Glacier, Lang- tang Himal, Nepal, from 1982 to 2009. Ann. Glaciol. 54, 157–162. https://doi.org/10.3189/2013AoG64A111 2013.

Sunako, S., Fujita, K., Izumi, T., Yamaguchi, S., Sakai, A., Kayastha, R.B., 2023. Up-glacier propagation of surface lowering of Yala glacier, Langtang valley, Nepal Himalaya. J. Glaciol. 69 (274), 425–432.

Taylor, C., Carr, J.R., 2019. Supraglacial pond evolution in the Everest region, central Himalaya, 2015-2018. In: *Supraglacial Pond Evolution in the Everest Region, Central Himalaya, 2015&Ndash;2018, March*, 1–33.

Thakuri, S., Salerno, F., Smiraglia, C., Bolch, T., D'Agata, C., Viviano, G., Tartari, G., 2014. Tracing glacier changes since the 1960s on the south slope of Mt. Everest (central Southern Himalaya) using optical satellite imagery. Cryosphere 8 (4), 1297–1315. https://doi.org/10.5194/tc-8-1297-2014.

Thompson, S., Benn, D.I., Mertes, J., Luckman, A., 2016. Stagnation and mass loss on a Himalayan debris-covered glacier: processes, patterns and rates. J. Glaciol. 62, 467–485.

Watson, C.S., Quincey, D.J., Carrivick, J.L., Smith, M.W., 2016. The dynamics of supraglacial ponds in the Everest region, central Himalaya. Glob. Planet. Chang. 142, 14–27.

Wester, P., Mishra, A., Mukherji, A., Shrestha, A.B., 2019. The Hindu Kush Himalaya assessment: mountains, climate change, sustainability and people. In: The Hindu Kush Himalaya Assessment: Mountains, Climate Change, Sustainability and People. Springer Nature. https://doi.org/10.1007/978-3-319-92288-1.

Zemp, M., Frey, H., Gärtner-Roer, I., Nussbaumer, S.U., Hoelzle, M., Paul, F., Vincent, C., 2015. Historically unprecedented global glacier decline in the early 21st century. J. Glaciol. 61 (228), 745–762.

Zhang, T., Wang, W., An, B., Wei, L., 2023. Enhanced glacial lake activity threatens numerous communities and infrastructure in the Third Pole. Nat. Commun. 14 (1). https://doi.org/10.1038/s41467-023-44123-z.

Zheng, G., Allen, S.K., Bao, A., et al., 2021. Increasing risk of glacial lake outburst floods from future Third Pole deglaciation. Nat. Clim. Chang. 11, 411–417. https://doi.org/10.1038/s41558-021-01028-3.